The Thesis Committee for Baolin Li
Certifies that this is the approved version of the following thesis:

Study on House-level Microgrids and Their Power Electronics

APPROVED BY
SUPERVISING COMMITTEE:

Supervisor:

Ross Baldick

Surya Santoso

Study on House-level Microgrids and Their Power Electronics

by

Baolin Li, B.S.; B.Eng.

Thesis

Presented to the Faculty of the Graduate School of

The University of Texas at Austin

in Partial Fulfillment

of the Requirements

for the Degree of

Master of Science in Engineering

The University of Texas at Austin

May 2017

Acknowledgements

First I would like to thank Professor Baldick for his supervision through my two years of study, and his revising on my thesis. I would also like to thank Professor Santoso for spending his time reading my work.

In addition, I would like to thank Dave Tuttle and Hunyoung Shin for their previous work in this area. I would like to thank Pecan Street Inc for providing the data for research.

Finally, I would like to thank my parents for their constant support.

Abstract

Study on House-level Microgrids and Their Power Electronics

Baolin Li, MSE

The University of Texas at Austin, 2017

Supervisor: Ross Baldick

This thesis introduces the concept of microgrid, and analyzes the capability for Plug-in Electric Vehicles (PHEV) and photovoltaics (PV) to support a residential load during the time when the utility grid has a power outage. A microgrid system model is introduced and simulations have demonstrated the performance of this microgrid in a grid outage. The possible power electronics interfaces in this microgrid configuration is investigated and compared. Several power electronics converters are introduced and simulated to realize different forms of power conversion. The system model of a DC-DC buck converter is formed, and a possible frequency compensator has been designed and simulated for it. This thesis has introduced the feasibility of a house-level microgrid in its theoretical backup performances, hardware implementations and control.

Table of Contents

List of Tables ix

List of Figures x

Chapter 1 Introduction 1

1.1 Background 1

1.2 Features of Microgrids 2

1.3 Motivations 3

1.4 Literature Review 4

1.4.1 Microgrid Case Study 4

1.4.2 Plug-In Vehicle to Home System Study 4

1.4.3 Medium Voltage DC and High Frequency AC System Architectures 6

1.4.4 Overview on DC Distribution Systems 6

1.5 Thesis Objectives 7

Chapter 2 V2H System Distributed Generations 9

2.1 Introduction 9

2.2 Plug-in Hybrid Electric Vehicles 9

2.2.1 From Conventional Vehicles to PHEVs 9

2.2.2 PHEVs in the Market 10

2.2.3 PHEV's Power Interface 12

2.3 Photovoltaic Panels 13

2.3.1 Panel Model 13

2.3.2 Panel Power Inverter 16

Chapter 3 Simulations of a V2H System 17

3.1 Introduction 17

3.2 System Model 17

3.2.1 Load and PV Profile 17

3.2.2 Scenario Description 17

3.2.3 Simulation Scheme 18
3.3 Simulation Results 20
3.3.1 Backup Duration 20
3.3.2 PV Spillage 21
3.3.3 One Particular Backup Event 21
Chapter 4 Power Electronics Interfaces in V2H System 24
4.1 Introduction 24
4.2 Interfaces in DC and AC Microgrid Configuration 24
4.2.1 AC Distribution Microgrid 24
4.2.2 DC Distribution Microgrid 25
4.2.3 Comparisons between DC and AC Configurations 27
4.3 DC/DC Converter Models 28
4.3.1 Buck Converter 28
4.3.1.1 Circuit Topology 28
4.3.1.2 Buck Converter Simulation 29
4.3.2 Boost Converter 31
4.3.2.1 Circuit Topology 31
4.3.2.2 Boost Converter Simulation 32
4.3.3 Other DC Converter Topologies 33
4.3.3.1 Buck-Boost Converter 34
4.3.3.2 Cuk Converter 34
4.3.3.3 Bi-directional Converter 35
4.4 DC/AC Converter Models 35
4.4.1 Rectifier 35
4.4.1.1 Circuit Model 36
4.4.1.2 Rectifier Simulation 36
4.4.2 Power Inverter 39
4.4.2.1 Circuit Model 39
4.4.2.2 Inverter Simulation 40

Chapter 5 Power Electronics Control in V2H System 45
5.1 Introduction 45
5.2 Introduction to Frequency Compensation 46
5.3 Compensator Types 49
5.3.1 Lead Compensator 49
5.3.3 Lead-lag Compensator 54
5.4 Control Application in Power Electronics 55
5.4.1 Converter Transfer Function 56
5.4.2 Lead-lag Compensator Design 59
5.4.3 Buck Converter Closed-loop Simulation 60
5.5 Hardware Implementations 62
Chapter 6 Thesis Summary 63
6.1 Conclusions 63
6.2 Future Work 63
References 65

List of Tables

Table 1. PHEVs in the market. 11

List of Figures

Figure 1. U.S. air pollution portions from power plants 1
Figure 2. A Microgrid Architecture Exemplar 3
Figure 3. PHEV pictures 11
Figure 4. SAE J1772 Connector 12
Figure 5. Equivalent circuit of a PV module 13
Figure 6. I-V and P-V curves of a PV in UT Austin 15
Figure 7. PV inverter schematic diagram 16
Figure 8. Simulation scheme 19
Figure 9. V2H backup duration throughout a year 20
Figure 10. PV spillage in every simulation 21
Figure 11. Load and PV profile in this backup event 22
Figure 12. PHEV behavior in this backup event 22
Figure 13. Simple representation of a typical V2H microgrid 25
Figure 14. Classified AC and DC loads 26
Figure 15. Simple representation of a DC Microgrid 26
Figure 16. Input and output voltage from a switching MOSFET 28
Figure 17. Topology of a basic buck converter 29
Figure 18. Simulation circuit of a buck converter 30
Figure 19. Output response to change in duty ratio 30
Figure 20. Output response to change in load 30
Figure 21. Topology of a boost converter 31
Figure 22. Simulation circuit of a boost converter 32
Figure 23. Output response to change in duty ratio 33

Figure 24. Output response to change in load....33
Figure 25. Topology of a buck-boost converter....34
Figure 26. Topology of a Cuk converter....34
Figure 27. Topology of a bi-directional converter....35
Figure 28. Rectifier with thyristor control....36
Figure 29. Simulation circuit of a controlled rectifier....37
Figure 30. Firing angle at 0°, average output voltage is 62.04V....37
Figure 31. Firing angle at 60°, average output voltage is 43.55V....38
Figure 32. Firing angle at 120°, average output voltage is 12.89V....38
Figure 33. Single phase inverter. Source: Figure 33 is from [30]....39
Figure 34. Waveforms of unipolar SPWM....41
Figure 35. Output voltage V_{AB}....42
Figure 36. Spectrum analysis of output V_{AB}....42
Figure 37. Output voltage V_{AB} with filter....43
Figure 38. Spectrum analysis of output V_{AB} with filter....44
Figure 39. Charging profile of a Li-ion battery....45
Figure 40. Closed-loop block diagram....46
Figure 41. Bode plot of the example system....47
Figure 42. Closed-loop step response when phase margin is 18°....47
Figure 43. Bode plot comparison of system with and without compensation....48
Figure 44. Closed-loop step response....49
Figure 45. Bode plot of the lead compensator....50
5.3.2 Lag Compensator....51
Figure 46. Bode plot for a lag compensator....52
Figure 47. Bode plot comparison of system with and without compensation....53

Figure 48. Closed-loop step response 53
Figure 49. Bode plot of a lead-lag compensator 55
Figure 50. Closed-loop control of a DC/DC converter 55
Figure 51. Bode plot of example buck converter 58
Figure 52. Closed-loop step response of example buck converter 58
Figure 53. Bode plot of the lead-lag compensator 60
Figure 54. Bode plot of system with and without compensation 61
Figure 55. Closed-loop response of system with and without compensation 61
Figure 56. Lead compensator circuit 62

Chapter 1 Introduction

1.1 BACKGROUND

In regions outside of US and EU, it is a general trend that the electricity consumption keeps rising. The traditional generation resources, such as coal and oil, are causing a lot of issues for our environment. These resources produce large amount of carbon dioxide, which traps heat in the atmosphere to cause global warming. Also, the coal and oil-fired power plants emit harmful pollutants including mercury, non-mercury metallic toxics and acid gases as we can see from the figure below.

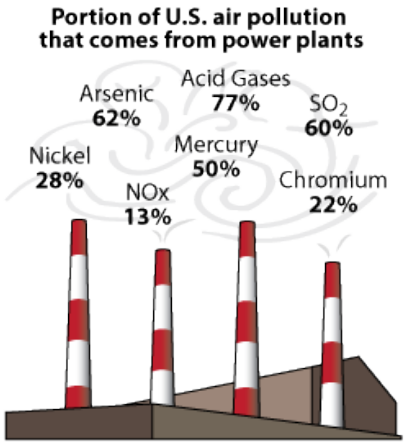

Figure 1. U.S. air pollution portions from power plants. Source: Figure 1 is from [1].

With the proposal of the smart grid, which is a power system that incorporates various techniques of control, automation, communication and monitoring, more renewable energy can be integrated into the grid. Besides large scale renewable plants of wind generation, solar energy is increasingly being embedded into electricity distribution networks worldwide on the customer side. Along with other customer-side generations such as microturbines, gasoline generators and natural gas generators, they are called

distributed generation (DG) units with capacities typically ranging from 1kW to 100MW. Customers using DG can have a higher degree of freedom to power their facilities at any time, or even inject power to the grid [2][3]. With some distributed generation, the customer can form a small local system called microgrid.

1.2 FEATURES OF MICROGRIDS

The main parts of a microgrid are the interconnected loads and the distributed generation. The interconnected generation and load is usually attached to a utility grid but is also able to function independently. Implementations of power electronics and sensors are required to provide proper monitoring and control.

The feature of a microgrid is that it can operate independently in "off-grid" mode or as a smaller subset of a utility grid in "grid-tie" mode. In normal conditions, there is an energy manager that decides the amount of power to draw or inject to the utility grid. A static transfer switch is an electrical device that when closed allows instantaneous transfer of power source to load. If there is a fault in the grid, it will switch the microgrid to off-grid mode to help maintain the power level for customer load [4]. The size of a microgrid can be flexible: it can be a customer's own house with his own DG, or a large military base.

Figure 2 shows an example of microgrid architecture: The whole microgrid is connected to the utility grid by some power electronics interfaces that can switch operating modes; the central yellow area works as the "brain" to control the collection and distribution of power; the distributed energy resources (DER) here include wind generators, PV modules, microturbines and fuel cells which are connected to the microgrid power distribution area; the power generated from DER will then be supplied to local loads, energy storages and, in some cases, the grid.

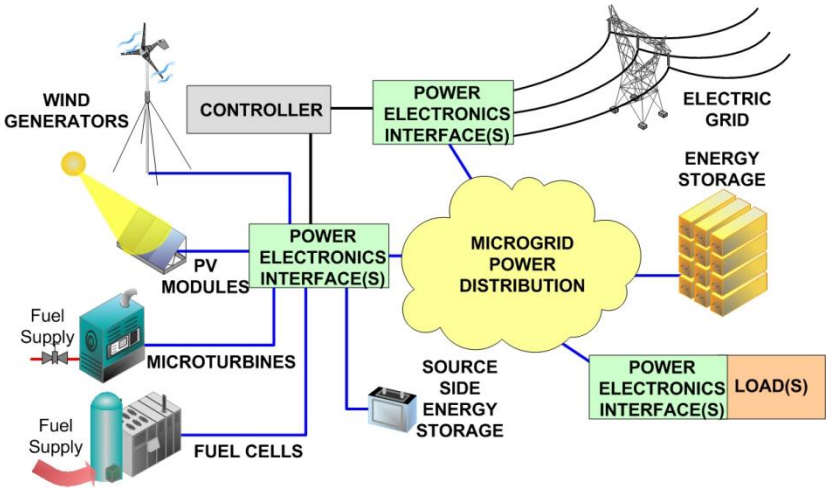

Figure 2. A Microgrid Architecture Exemplar. Source: Figure 2 is from [5].

1.3 MOTIVATIONS

The study of microgrid is important because:

- In areas that have abundant renewable energy such as solar and wind power, the microgrid can be very reliable and cost-effective for an environmentally friendly system;
- Microgrid provides the capability of powering the customers during an electricity outage. With proper control algorithms, customers can maximize the power supply duration and remain energized until the recovery of the grid;
- Microgrid makes it possible for individual customers to sell electricity back to the grid and places the consumer in a better bargaining position against large generation and network companies; and
- Aside from individual houses, microgrid has an extensive area of applications in utilities such as hospitals, where a power outage or disturbance would result in severe losses to the public.

1.4 LITERATURE REVIEW

1.4.1 Microgrid Case Study

Reference [6] has fully demonstrated a microgrid that was constructed in Sendai, Japan and how the microgrid helped during an earthquake power outage. The distributed energy resources were one phosphoric acid fuel cell, two gas turbines and a PV array. The main energy source in island operation was natural gas. The waste heat from gas engine were also delivered to residents for heating.

The load was divided into 5 classes (DC, A, B1, B3 and C with priority from high to low) according to the power quality requirements. When the earthquake occurred, the utility grid was shut down for 3 days, during which the microgrid was operating in island mode. The gas engine accidentally stopped working because of control issues, so only DC load, class A and B1 load were served with the battery and PV. Later on, with battery storage decreasing, the voltage level cannot satisfy A and B1 load so only DC load was supplied. After 21 hours of operation, gas engine was fixed and restarted, all classes of loads were fully supplied. Also, the importance of power diversity and backup equipment was discussed, since some loads were still supplied given the abnormal operation of gas engine.

1.4.2 Plug-In Vehicle to Home System Study

The author of [7] has modeled a Vehicle-to-Home(V2H) system composed of a PHEV generator, battery, PV and load. During off-grid operation, energy production priorities from high to low are: PV, battery, engine generator until the gasoline is exhausted. The battery charge/discharge efficiency was obtained and the energy conversion ratio (ECR) from gasoline to electricity was measured for a Chevrolet Volt model.

This paper also introduced some key power electronics interfaces and control algorithms needed for a V2H system. In the off-grid mode backup duration simulations, the control algorithm used was to allow battery State of Charge (SoC) drop to a lower bound (0%), then the generator charges it to an upper bound (100%) and repeat. However, a V2H system with PV would have PV spillage when the battery was charged too full to store the solar energy. Two more optimal strategies were proposed by the author: one was to lower the SoC upper bound, the other was to cease load supporting before battery was fully depleted so that the remaining charge can restart PV operation and then power the load, which has the potential to indefinitely provide power. The backup duration can be further extended with better demand side response.

Reference [33] has proposed an optimization model in a V2H microgrid to maximize the backup duration during a grid outage. The author suggested that if we use the PHEV generator to directly supply the house load, the battery charging and discharging power loss can be avoided, but the generator has a poor efficiency at a residential-level power output. Charging the battery at a high-efficiency generator output range should be more beneficial than serving the load at a low-efficiency range. In the algorithm proposed, extra PV power is used to charge the battery; If load is greater than PV generation, the battery is discharged; For the remaining unsatisfied load, the generator will directly serve the load if it is large enough, or serve the load while charging the battery if the load is small. The author also extended his model to a Vehicles-to-Homes (Vs2Hs) model which enables power backup to homes using shared distributed generation units.

1.4.3 Medium Voltage DC and High Frequency AC System Architectures

The University of Texas at Austin Center for Electromechanics (UT-CEM) has developed a navy ship microgrid test bed at MW power levels [8]. The system is configured around a central 2 kV DC bus that incorporates multiple power sources as well as active and passive loads. The sources include two independent conventional utility power supplies and high frequency generators directly driven from gas turbine prime movers. The power electronics modules include a passive full bridge diode rectifier and an active IGBT controlled rectifier, as well as a variable frequency drive that can output frequencies up to 300Hz with power from DC bus. This microgrid features a variety of resistive, inductive and switched dynamic loads. Two types of faults that may happen in this microgrid has been simulated: one simulates a mechanically well supported power system that initiates an arc due to failure of a conductor or connector, the other simulates an energized cable that breaks and falls off accidentally. This paper has provided a real case of microgrid that can use both DC and AC as the main power distribution bus.

1.4.4 Overview on DC Distribution Systems

Reference [9] has given an integrated background in the field of DC power systems, including the reasons, challenges, proposed solutions, standardization efforts and applications.

Reasons for DC systems has been explained as following:

- Due to the stunning advent of semiconductor technology and power electronics converters, DC power can be utilized easier than before.
- Using DC bus system means removing one rectifier and one power factor correction (PFC) stage for DC loads, which takes a large portion of today's consumer loads.

- Some renewable energy sources are natively DC, such as photovoltaic and fuel cells. Also, most of the storage elements are purely DC, such as battery and ultra-capacitors.
- DC power is a reliable form of energy to be supplied to data centers, which are very sensitive to harmonics in AC systems due to the existence of nonlinear loads.
- For electric vehicles, researchers believe that there should be a DC bus at which EV batteries and any DG units should be integrated [10].

In [11], the authors have reviewed the past researches in the loss comparisons between the AC and DC distribution systems, and concluded that in offshore regions, DC systems have lower losses over a wide range of operating voltages, load currents and transmission distances. In [12], it was suggested that DG-based DC microgrids have a disturbing impact on utility grids due to the perturbations of their power generation, and the solution could be a synchronverter, an inverter with modified control to emulate the characteristics of a synchronous machine. In terms of DC system protections, several publications have proposed various solutions, such as ultra-fast hybrid DC circuit breakers [13], adding shunt diode/capacitor branch to the plug [14], and fast DC switches [15].

1.5 THESIS OBJECTIVES

This thesis aims at studying the microgrid in the level of a house with PV and Plug-in Hybrid Electric Vehicle (PHEV) generation. The following topics will be covered in the upcoming chapters:

- Basic modeling of distributed generations
- Simulation of a vehicle-to-home microgrid
- Basic power electronics interfaces and circuit topologies

- Power electronics control algorithms and simulations

All the topics will contribute towards establishing a house-level microgrid from its concept to real hardware implementations.

Chapter 2 V2H System Distributed Generations

2.1 INTRODUCTION

The Vehicle-to-home (V2H) system discussed in this thesis is composed of a PHEV, a PV panel and the residential load. In the scenario of "off-grid" operation, all the solar power will be used to supply the load and during the times when bad weather or a large load occurs, the PHEV will compensate for the positive net load, feeding power to the house load when its electric motor is stationary. This proposal is feasible as long as the peak load does not exceed the power capacity of the PV and PHEV.

In this chapter, the PHEV is introduced in terms of its advantage over conventional vehicles, its recent development in the market and how it shall be connected to the residential loads as a distributed energy resource. As for PV panel, its basic operation principle, circuit and mathematical model, maximum power point tracking, and power interface are presented.

2.2 PLUG-IN HYBRID ELECTRIC VEHICLES

2.2.1 From Conventional Vehicles to PHEVs

A conventional vehicle with a gasoline powered engine is very inefficient in using the fuel we put in the tank to moving driving the car or running useful accessories such as air conditioning. According to a study by the U.S Department of Energy [17], around 70% of the fuel's energy is lost in the engine, primarily as heat. Together with parasitic losses (e.g., water pump, alternator), drivetrain losses and idle losses, the power to the wheels takes up only 18-25% of the total chemical energy.

As for a hybrid electric vehicle (HEV), it combines the benefits of a gasoline engine and electric motors, owing to several new technologies. The technology of

regenerative braking makes use of the forward motion of the wheels during braking to turn the motor in reverse, which can generate electric power while slowing down the vehicle. Another technology is electric motor assist, which chooses the more efficient engine to be used in various situations. For instance, when the vehicle moves at low speeds, the gasoline engine will be shut off and the electric motor operates alone.

From the same study in [17], a hybrid vehicle has slightly less engine loss and negligible idle loss. Also, 5-9% of the energy is recovered by regenerative braking, leading to 27-38% of the input energy delivered to the wheel power, which is 10% higher than a conventional vehicle. A PHEV is basically the same structure as a HEV, with a new capability of grid charging. This new feature also, in principle, allows customers to use their vehicles to provide power to their residential load during a blackout or supply the grid in a summer afternoon.

2.2.2 PHEVs in the Market

Given the PHEVs' advantages over traditional vehicles and increasing public acceptance, more and more automobile manufacturers are vigorously increasing their investment on electric vehicles. For example [18], the Chevrolet Volt is a PHEV manufactured by General Motors. In October 2015, the global sale has passed the 100,000-unit milestone, with the United States being the largest market, with over 84,600 Volts delivered. The Volt operates as a pure battery electric vehicle (BEV) until its battery charge state drops to a predetermined threshold. After dropping to the threshold, its internal combustion engine will serve as an electric generator to extend the range. This operation characteristic will be used for simulations in Chapter 3, where the battery discharges to serve the residential load instead of the electric motor.

Some of the available PHEVs in the market are listed in the table below, with the range from economical vehicles to luxury ones.

model	manufacture	release date	battery size (kWh)	charging rate (kW)	EPA range (miles)	electric motor power (kW)	combined power (horsepower)	MSRP (USD)
A3 E-Tron	Audi	Jan 2016	9	3.3	16	75	204	37900
i8	BWM	Jan 2014	7	3.3	25	96	357	137000
2016 Volt	Chevrolet	Jan 2016	18	3.6	53	NA	149	34000
Prius Plug-in Hybrid	Toyota	Jan 2012	4	3.3	11	60	134	30800
Sonata Plug-in	Hyundai	May 2015	10	3.3	27	50	202	35400
Fusion Energi	Ford	Jan 2013	7	3.3	20	88	188	35600

Table 1. PHEVs in the market. Source: Table 1 is from manufacturer websites.

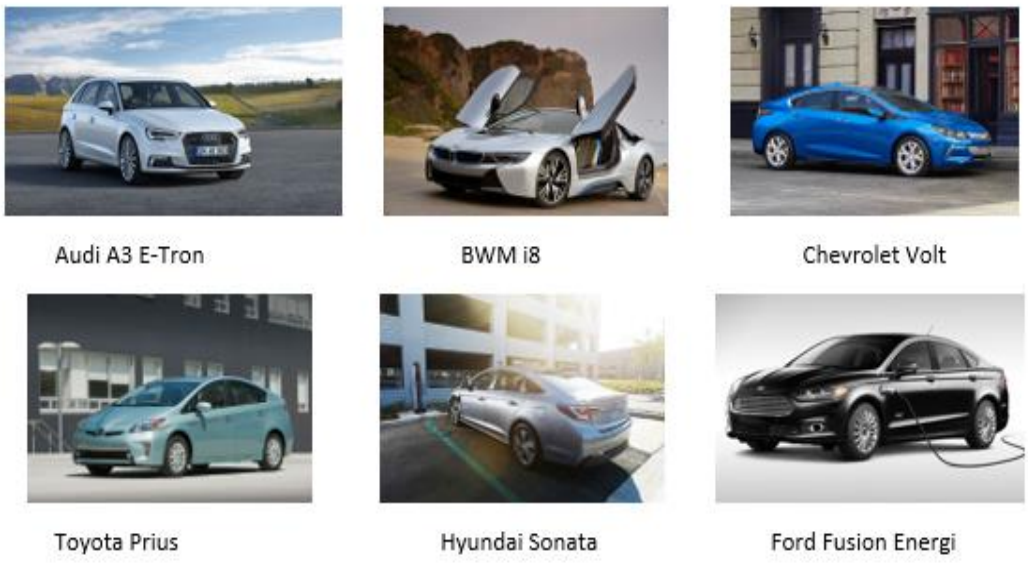

Figure 3. PHEV pictures. Source: Figure 3 is from manufacturer websites.

2.2.3 PHEV's Power Interface

The North American standard interface for electric vehicles is the SAE J1772 connector [19]. It has various power capacities for both AC and DC interfaces. The AC interface has two charging levels, with level 1 being 120V 1.92kW single phase charging, and level 2 being 240V 7.68kW/19.20kW split phase charging. As for DC interface, it is based on the AC connector with additional DC and ground pins, which can support 200-450V DC charging. It also has two levels, with 36kW for level 1 and 90kW for level 2, which are significant improvements compared to the AC interface. Figure 4 shows a typical connector that is being widely used, and the two pins at the bottom are the additional DC and ground pins.

Figure 4. SAE J1772 Connector. Source: Figure 4 is from [20].

According to [24], to supply the residential AC power, Nissan has developed a Leaf-to-Home system that allows customers to supply their homes with the energy stored in a Nissan LEAF's battery. Household power can be supplied from a Nissan LEAF lithium-ion battery by installing a PCS (Power Control System) connected to the

household's distribution board. The PCS handles the power conversion and control of the amount of power supply. Other car models such as Mitsubishi Outlander and Toyota Prius also have the feature of Vehicle-to-Home discharging.

2.3 PHOTOVOLTAIC PANELS

2.3.1 Panel Model

A solar panel can convert incident sunlight into electricity by photovoltaic conversion. Each individual cell in the panel is a large-scale semiconductor diode that allows light to penetrate into the p-n junction region. Photons are absorbed in the junction, generating excess electrons and holes. When the electrons flow through an external circuit, then power is produced.

In [21], the PV module is modeled as the equivalent circuit below, where the cell is equivalent to a current source in parallel with a diode and a shunt resistor, together with a series resistor. The series resistance represents the internal resistance depending on the p-n junction depth, the impurities and the contact resistance. The shunt resistance conducts the leakage current to ground.

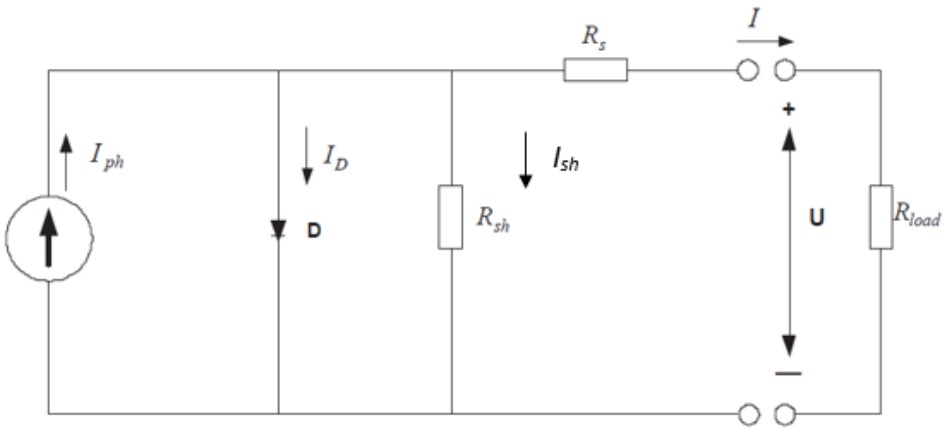

Figure 5. Equivalent circuit of a PV module. Source: This figure is from [21]

From the circuit, the output current can be represented as

$$I = I_{ph} - I_D - I_{sh} \ldots (2.1)$$

where the shunt current is

$$I_{sh} = \frac{V_{sh}}{R_{sh}} = \frac{U + I \cdot R_s}{R_{sh}} \ldots (2.2)$$

The diode current is given by the Shockley diode equation as

$$I_D = I_s \cdot \left(e^{\frac{V_D}{n \cdot V_T}} - 1 \right) \ldots (2.3)$$

Where:

- Is is the reverse bias saturation current.
- VD is forward voltage across diode, which is also $U + I \cdot R_s$.
- VT is the thermal voltage, and
- n is the ideality factor.

By the approximation of ignoring leakage current, a simplified PV panel output I-V equation can be derived as

$$I = I_{ph} - A(e^{B \cdot U} - 1) \ldots (2.4)$$

where I_{ph}, A and B are the panel parameters that vary with panel characteristic and solar radiation. With measurements taken over the rooftop PVs on ECJ, UT Austin for a particular illumination level, the corresponding current and power against voltage curve is shown in Figure 6:

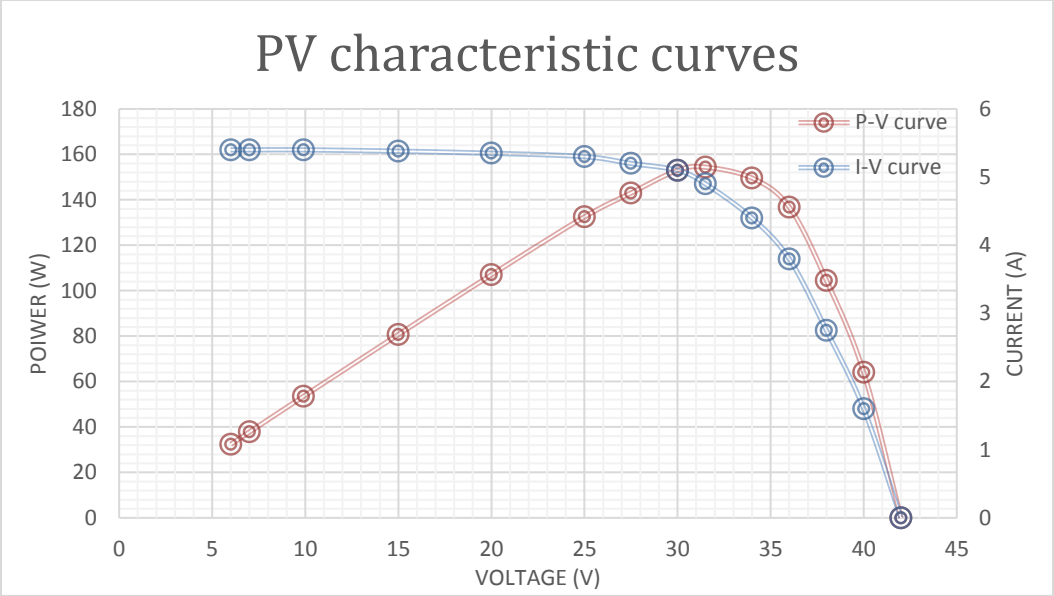

Figure 6. I-V and P-V curves of a PV in UT Austin

Using the Excel curve estimation, equation (2.4) can be explicitly filled to this case as

$$I = 5.457 - 1.257\times10^{-3}\times(e^{0.1999U} - 1) \ldots (2.5)$$

As we can see from the P-V curve, there is a point at which the output power is maximized. The users always expect their PVs to operate around this point, and this can be accomplished by the maximum power point tracking (MPPT) technology. Over the years, many MPPT methods have been developed and implemented, including exemplar techniques of hill climbing, fuzzy logic and neutral network control, dP/dV or dP/dI feedback control. The detailed overview of these methods can be found in [22]. In real life cases, to maximize production, the PV panel should have the capability of not only adjusting its orientation for the maximum radiation, but also tracking the maximum power point.

2.3.2 Panel Power Inverter

The PV panel requires a solar inverter to convert a variable DC power into a fixed frequency AC power. Normally, if a PV feeds power back to the grid, then we need a grid tied inverter, which has the function of phase matching and quick disconnection when the grid shuts down; if a PV is used in an isolated system, an ordinary stand-alone inverter can manage the power conversion.

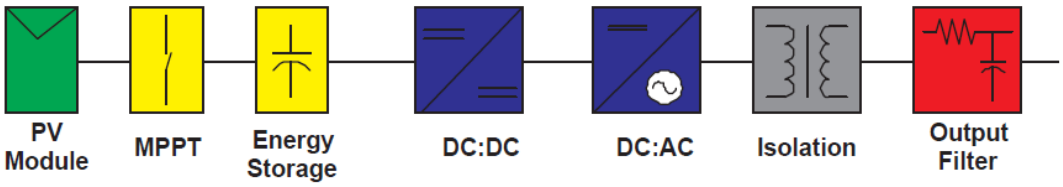

Figure 7. PV inverter schematic diagram. Source: This figure is from [23].

A typical PV inverter should include the components shown in Figure 7, where the PV output power is maximized by the MPPT circuit into an energy storage capacitor. The DC-DC converter can be a flyback or a forward converter that steps the voltage up to a fixed level and provides galvanic isolation. The isolation transformer after the inverting stage rejects the DC components and the output low pass filter can restrict the high frequency harmonics from going into the residential load.

Chapter 3 Simulations of a V2H System

3.1 INTRODUCTION

With the V2H microgrid described in the previous chapters, it is still not guaranteed that the system can operate in island mode for a period that is considered as acceptable to customers. In this chapter, a particular scenario is set up for the microgrid with the AC distribution system, and the simulation of the microgrid power backup event in a whole year will be done. Based on the simulation, it can be determined if the V2H system is feasible in a real-life case. The results will also be used later for comparison with the DC distribution system.

3.2 SYSTEM MODEL

3.2.1 Load and PV Profile

The load and PV generation data were collected by Pecan Street Inc. in Austin. These data were taken from 20 houses at 1-minute intervals over the whole year of 2012. In this work, only one house's profile was randomly chosen and this profile will also be used in the DC distribution simulations in the following chapters. The PV profile is the PV power measured at the load side, which means that the PV inverter efficiency has been included. Therefore, the net load can be obtained by direct subtraction of load and PV power. One assumption in the simulation is that the PV and load power measured is the average power during the 1-minute interval.

3.2.2 Scenario Description

The simulation scenario is based on the research from [7], where the V2H system is isolated from the utility grid. A power backup is the process of using the PHEV

generator and PV to supply the load during a grid outage. The details are specifically introduced below:

1. Backup starting time: throughout the whole year, which is from day 1 to day 350 at 12 a.m., corresponding to minute 1,440 to minute 504,000 in the PV and load profile. The reason for skipping the last couple of days in the year is that there will not be enough data to support the simulation if the backup duration is longer than the remaining days in this year.
2. Conversion efficiency: 88%, which means that there is a 12% one-way energy loss when the battery is charged by the PV or discharges to serve the load.
3. Gasoline generator: at 1700rpm, the energy conversion ratio is 8.4kWh/gallon, which means one gallon of fuel is converted to 8.4kWh of electric energy in the battery. The initial gasoline in the tank is set at 17 gallons.
4. Battery: the battery size is 10.5kWh, with battery charge power of 12.4kW at 1700rpm. The maximum battery output power is 110kW, which can guarantee the load to be supplied. The battery is assumed to be fully charged initially.
5. Backup duration: when there is no gasoline and the battery charge is below a certain level (10%), the simulation ends, the total operation time is the backup duration.

3.2.3 Simulation Scheme

We run the backup process for every possible backup staring time and plot the backup duration against time, which means that the simulation should be repeated 350 times. Assuming when battery state of charge (SoC) is below 10%, the vehicle engine charges the battery to 90% SoC, since charging battery to no more than 90% can help

avoid more PV spillage. For each day of simulation, the operation scheme is shown below:

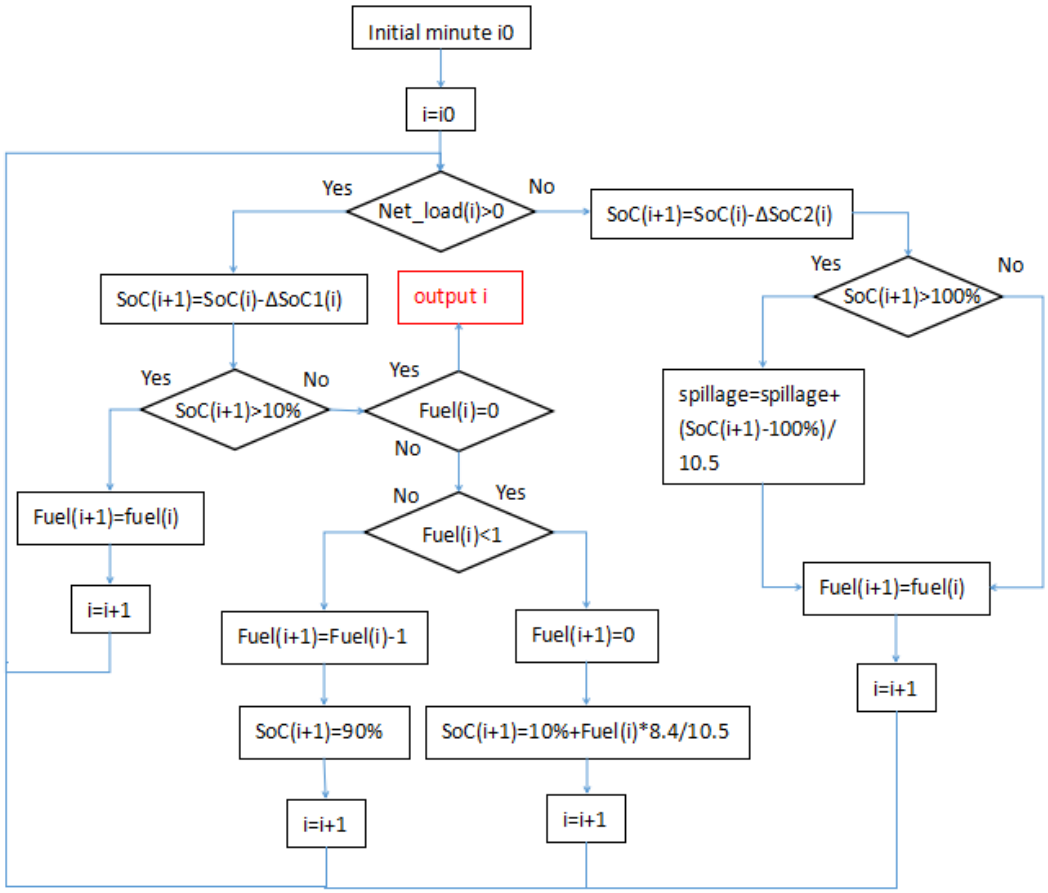

Figure 8. Simulation scheme

In this scheme, the final output i is the minute that the backup ended, when there is no gasoline remain and SoC is smaller than 10%. The units for net load and spillage is kW, for fuel is gallon. The term ΔSoC1 represents the change in SoC when battery discharges, specifically $\frac{Net\_load(i)}{88\%\times60\times10.5}$, while ΔSoC2 represents the change in SoC when battery gets charged by PV, which is the term $\frac{88\%\times Net\_load(i)}{60\times10.5}$. The spillage stands for the PV spillage when the battery is fully charged while the PV is still charging the battery. In

the judgement "Fuel(i) < 1", "1" represents the fuel needed to charge the battery from 10% to 90%, since $\frac{80\%\times 10.5}{8.4} = 1 \ \ (gallon)$.

3.3 Simulation Results

3.3.1 Backup Duration

The duration of the microgrid power backup is dependent on the start of the grid power outage. The figure below shows the backup duration against outage start date.

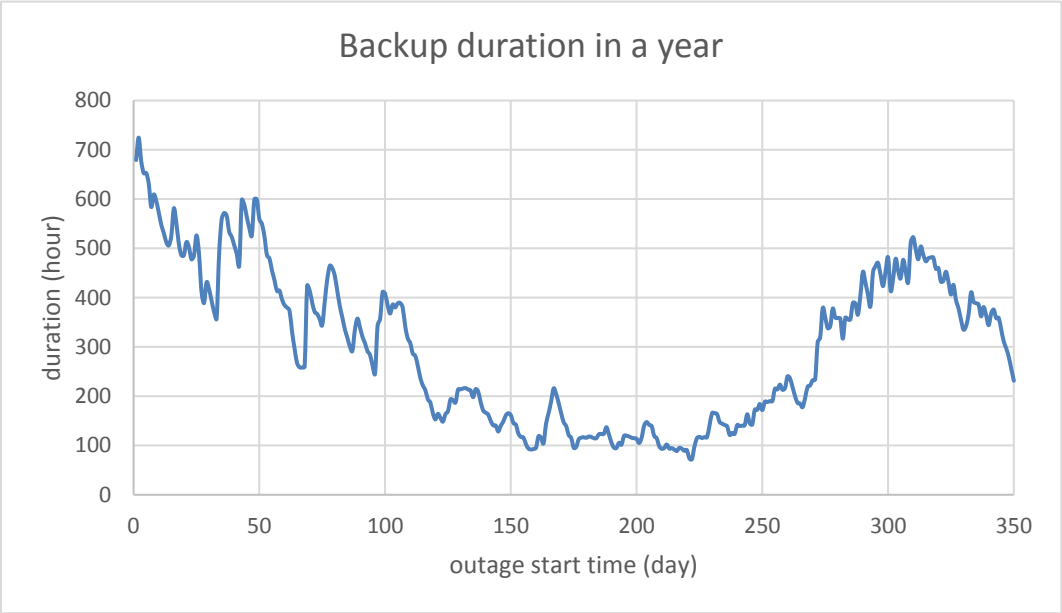

Figure 9. V2H backup duration throughout a year

From the simulation result, it can be concluded that the duration is relatively short between day 150 and day 250, which is approximately the time of summer. The shorter backup is expected in summer because normally load peaks occur during this season. The shortest backup time is roughly 100 hours, which is still typically enough time for the grid to recover from outage.

3.3.2 PV Spillage

It is possible that when the PHEV battery is already fully charged, the PV generation is still larger than the load, leading to PV spillage. The total spillage corresponding to every simulation is shown below:

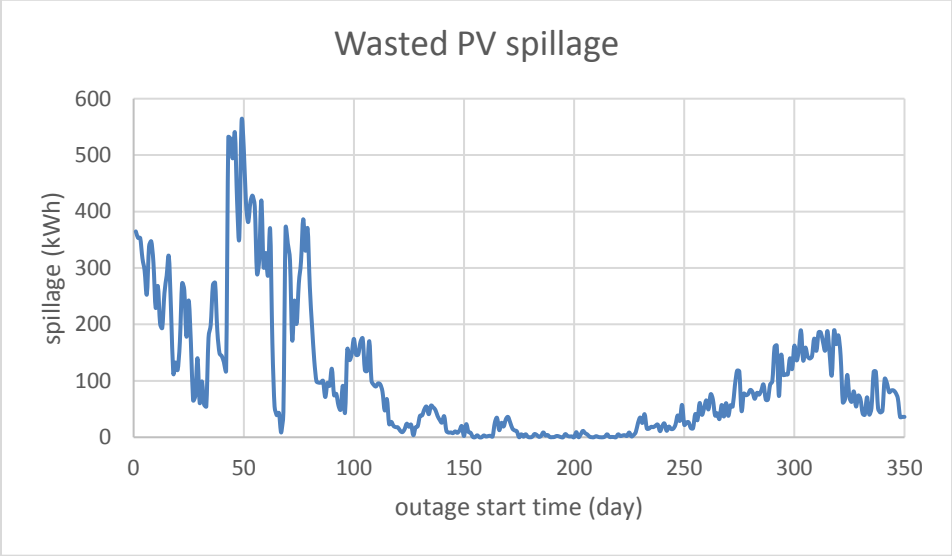

Figure 10. PV spillage in every simulation

As we can see, the PV spillage is very small in summer even though the solar radiation is large, which means that the load in summer is so large that even more PV generation cannot cancel it out. This is also consistent with the observation that the backup duration is so short in summer.

3.3.3 One Particular Backup Event

If we look into the details of one particular backup at a randomly chosen day 200, the backup duration is 113.73 hours, and PV spillage is 0. The load and PV generation as well as the PHEV behavior can be shown below.

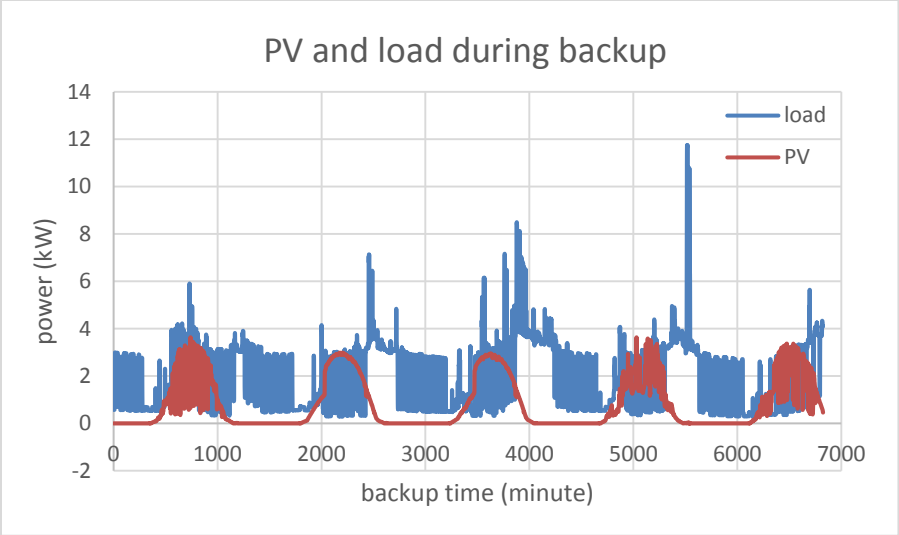

Figure 11. Load and PV profile in this backup event

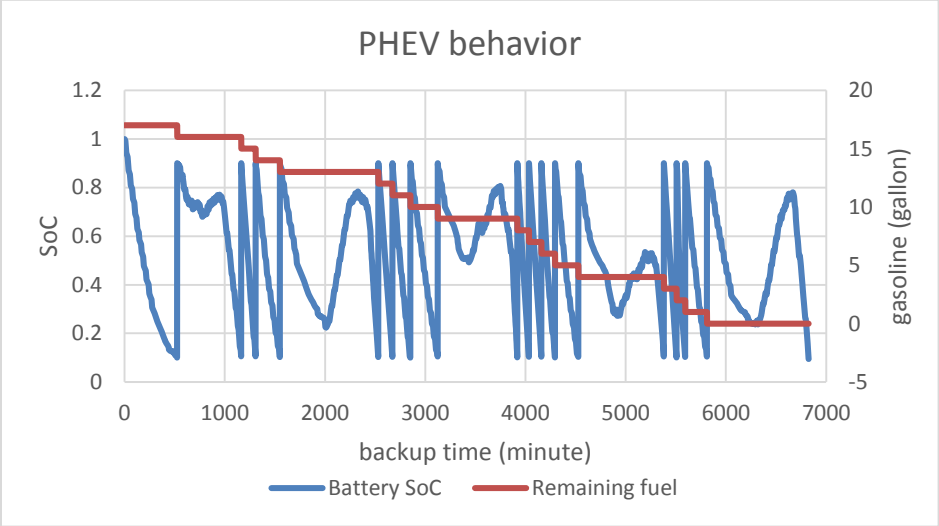

Figure 12. PHEV behavior in this backup event

In these two figures, we can see that the load is larger than PV generation for most of the backup time, and the battery has never reached a fully charged state, which is in accordance with the 0 PV spillage. During some times (e.g., at minute 2000) when

gasoline is not being consumed, the battery SoC still goes up, which is because of the charge from PV exceeding load.

From all the simulations above, a conclusion can be drawn that theoretically, the V2H microgrid is capable of supporting a residential load for a significant amount of time can be drawn.

Chapter 4 Power Electronics Interfaces in V2H System

4.1 Introduction

As was introduced in previous chapters, the configuration of a V2H microgrid has two distributed generation units: PV panel and PHEV generator. A lot of DC/DC and DC/AC conversion processes are taking place during an operation of the microgrid. Therefore, the power electronics modules are very important in building a microgrid.

In this chapter, the power electronics interfaces in both a DC and AC microgrid will be introduced, along with some basic power converter models such as rectifier, inverter and DC/DC converter.

4.2 Interfaces in DC and AC Microgrid Configuration

There are two possible configurations of a microgrid: one is with an AC distribution system, where both PV and battery energy are converted to AC first to flow in the house; the other is a DC microgrid, where loads are classified and power is distributed along a DC bus.

4.2.1 AC Distribution Microgrid

The first scenario is a typical Vehicle to Home (V2H) microgrid described in [7]. Under the assumption that one cannot drive the vehicle to fueling station during the backup and the load demand remains normal, the operation can be simulated with a given amount of gasoline and battery state of charge (SoC). The backup duration optimization can become a complicated problem when taking the gasoline generator efficiency, battery charging/discharging efficiency, PV generation, and loadshape into consideration. Figure

13 shows a simplified version of the microgrid, where the load includes both DC and AC load, and the load demand is the power taken directly out of the wall outlet.

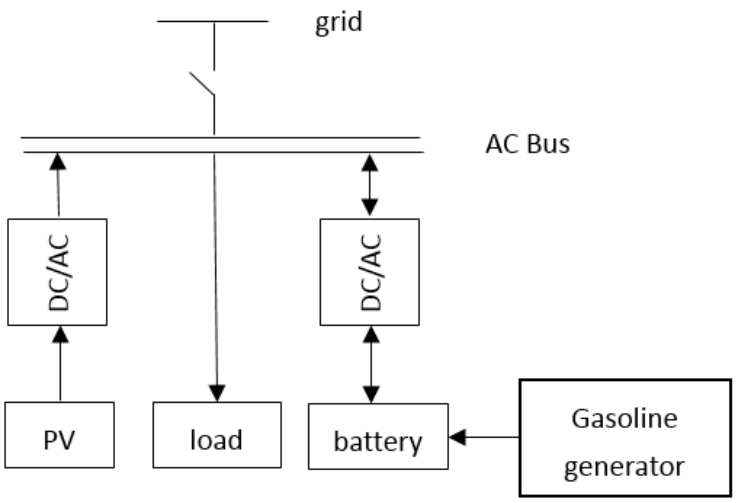

Figure 13. Simple representation of a typical V2H microgrid

4.2.2 DC Distribution Microgrid

For the loads in a residential house, a significant portion of them are native DC loads, such as laptop, LED lighting and television. Normally, a rectifier and DC-DC converter is included in the wall wart that plugs in the load to the outlet. Therefore, the load can be represented as below:

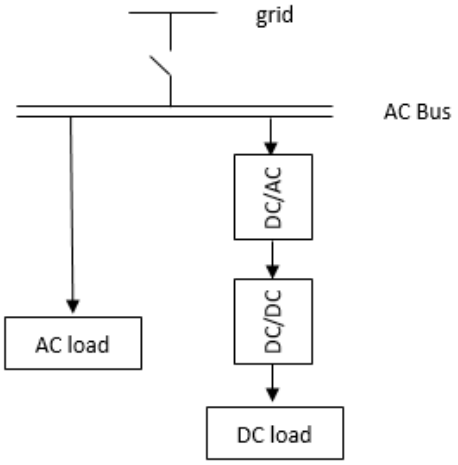

Figure 14. Classified AC and DC loads

After the load has been classified into AC and DC load, we can consider using a DC bus to interconnect the PV, battery and DC load because the two energy sources are supplying power in DC form [16]. A two-way rectifier/inverter will be needed to connect the DC bus and AC bus from the grid, then we can configure the system as Figure 15.

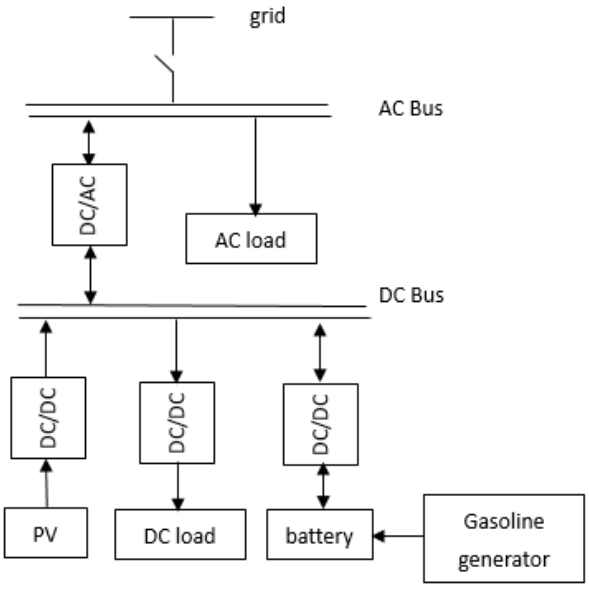

Figure 15. Simple representation of a DC Microgrid

4.2.3 Comparisons between DC and AC Configurations

The utility grids are using an AC system as a convention mainly because the power is generated in AC form and can be transmitted at high voltage using transformers. However, microgrid does not have these features. In this V2H system, the distributed generation units are DC in nature and power is not required to transmit at higher voltages to lower loss. Thus, it is worth comparing the two distribution systems.

The AC system configuration is less complicated. The DG units are connected to the distribution bus using DC/AC inverters and everything else is the same as the current in-house power distribution system. The set-up of DC configuration is more challenging because:

- Load classification is required to separate AC and DC loads
- An additional DC bus is added to serve the DC loads.
- Most appliance manufactures provide AC power adapters only. And
- there is a lack of standard for the DC bus and DC adapters.

However, there are more potential power losses in an AC configuration. The DC power generation must be converted to AC to flow in the system, then converted back to DC for consumption in these cases:

- When PV is used to charge PHEV battery, and
- when the power from battery and/or PV are used to serve DC load.

Overall, determining whether DC or AC microgrid is better for a house-level configuration is complicated and many trade-offs need to be considered based on aspects such as proportion of DC load, PV generation, difficulty of reconfiguration and on.

4.3 DC/DC Converter Models

4.3.1 Buck Converter

A buck converter is used to step a DC voltage down. In a DC microgrid, the DC bus is usually a high voltage bus. When using the DC bus to serve the DC load, for example, an LED light bulb with a 12V rating, a buck converter or a similar step down converter is needed to lower the voltage level.

4.3.1.1 Circuit Topology

Suppose there is a power MOSFET that keeps switching on and off with a period of T and duty cycle of D. A constant input voltage level will be chopped to a rectangular waveform. This process can be represented in Figure 16.

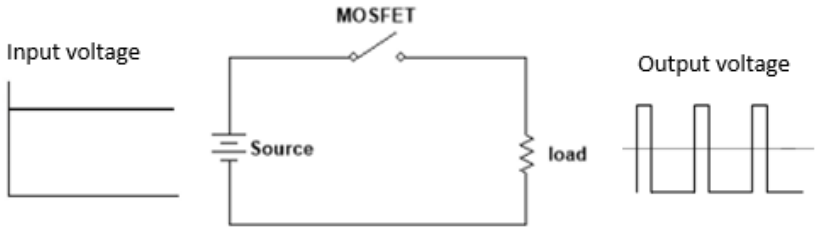

Figure 16. Input and output voltage from a switching MOSFET

When we look at the Fourier series of the output waveform, it will consist of a DC average bias and a series of sinusoidal waveforms. For example, when the duty cycle D=0.5, the Fourier series of the output square wave will be

$$V_{out}(t) = V_{DC-bias} + \frac{4}{\pi}\sum_{n=1,3,5\ldots}^{\infty}\frac{1}{n}\sin(\frac{n\pi t}{T}) \ldots (4.1)$$

However, this amount of harmonics is definitely not acceptable for a microgrid system. By applying an LC low pass filter at the output and adding a free-wheeling diode to allow current flow when the switch is off, a basic buck converter topology is built up.

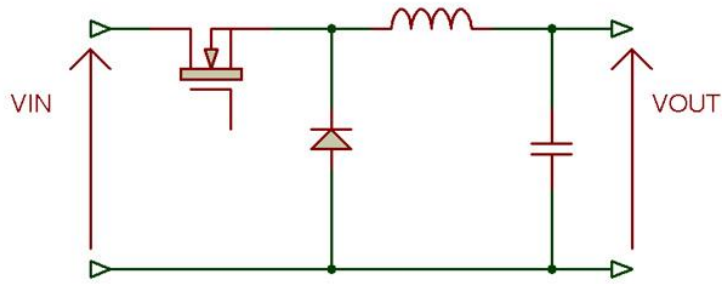

Figure 17. Topology of a basic buck converter. Source: Figure 17 is from [25]

The LC low pass filter will attenuate the output harmonics and make $V_{out} = V_{DC-bias}$. Since the DC bias is the average of the rectangular wave, we have this relationship:

$$V_{out} = DV_{in} \ldots (4.2)$$

By changing duty ratio D, we can change the output voltage to a desired value.

4.3.1.2 Buck Converter Simulation

A buck converter circuit model with a switching frequency of 10kHz has been built in Multisim for simulation. In the first simulation, the input voltage is 30V. The duty ratio D is changed from 0 to 0.8 with a step of 0.2. In the second simulation, the duty ratio is kept constant at 0.5, but the load resistance is changed from 2.08Ω to 5.55Ω.

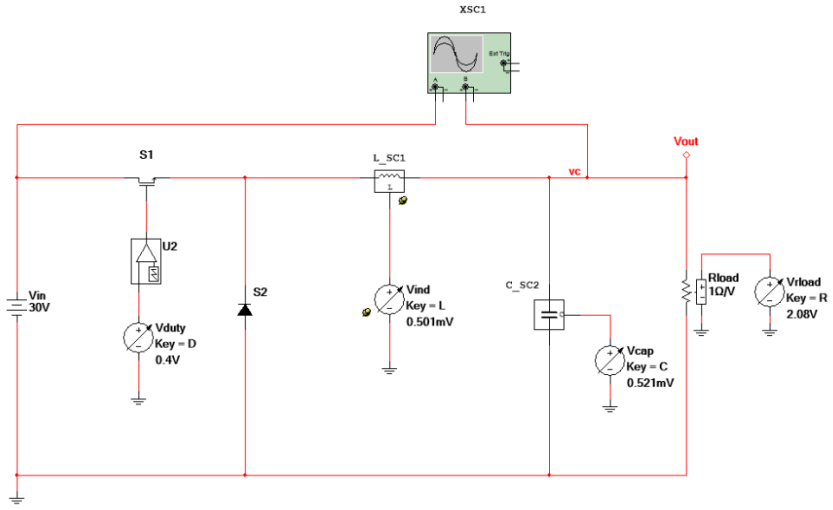

Figure 18. Simulation circuit of a buck converter

Figure 19. Output response to change in duty ratio

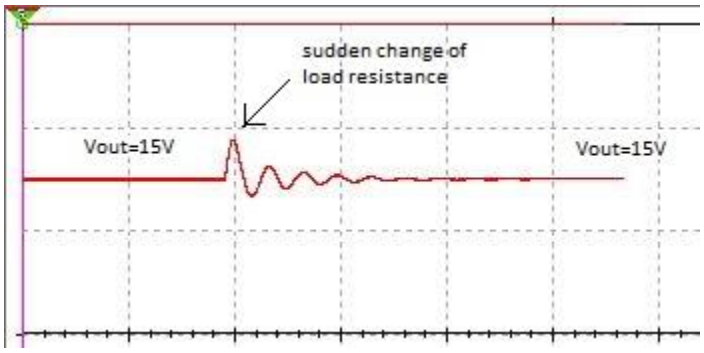

Figure 20. Output response to change in load

From the first simulation in Figure 19, we can see that the output and input satisfy equation (4.2). When the duty ratio is changed, the response takes some time to become stable and is very oscillatory with obvious overshoot. The second simulation in Figure 20 also shows a similar oscillatory response, but this time since the duty ratio is constant, the output voltage goes back to 15V eventually. These responses are understandable because the buck converter is operating in open-loop and there is no controller to modify its characteristics.

4.3.2 Boost Converter

A boost converter steps a DC voltage up. For example, when a PV panel with a 17V output rating feeds power to the DC bus, or when the DC bus is performing a 500V fast charging (SAE level 2 charging standard) to the vehicle battery, a boost converter or a similar step-up converter is needed.

4.3.2.1 Circuit Topology

The boost converter topology is very similar to that of a buck converter, with the positions of inductor, MOSFET and diode swapped.

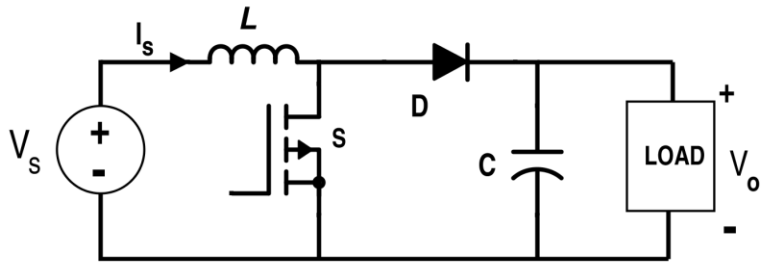

Figure 21. Topology of a boost converter. Source: Figure 21 is from [26]

When the MOSFET is switched on, the source keeps charging the inductor, energy is stored in L. Load is isolated from the input source during on time. When the

MOSFET is switched off, the energy stored in L is dumped into the load. This type of converter is called indirect converter because the source does not directly serve the load.

Equation (4.3) shows the relationship between output voltage and input voltage. It is derived by analyzing the current in inductor, and a detailed derivation can be found at [27].

$$V_{out} = \frac{V_{in}}{1 - D} \ldots (4.3)$$

4.3.2.2 Boost Converter Simulation

A boost converter circuit model has been built from component rearrangement of the buck converter. The MOSFET switching is still 10kHz. The input voltage is 10V. In the first simulation, the duty ratio D is changed from 0 to 0.6 with a step of 0.2. The duty ratio cannot be too close to 1 because it will make the output voltage too high. In the second simulation, the duty ratio is kept constant at 0.4, but the load resistance is suddenly changed from 2.08Ω to 5.55Ω.

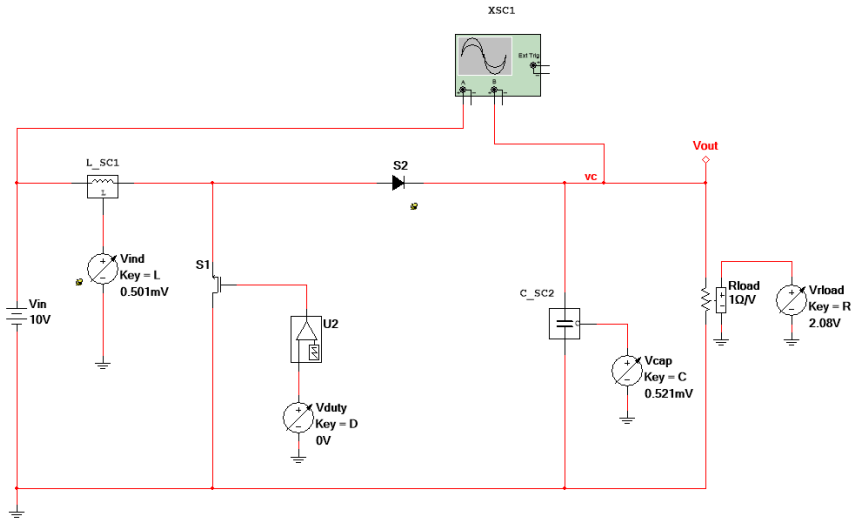

Figure 22. Simulation circuit of a boost converter

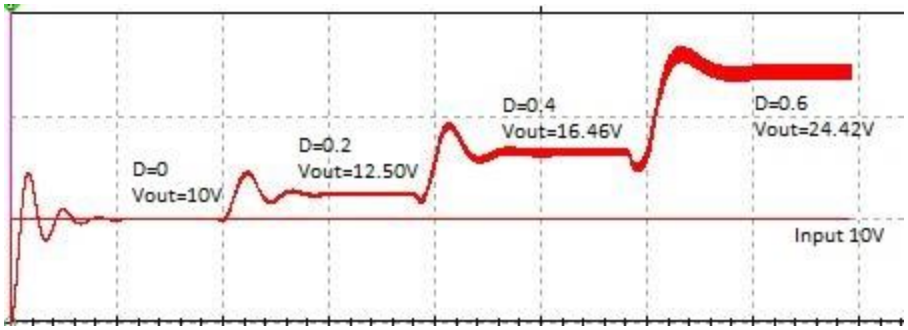

Figure 23. Output response to change in duty ratio

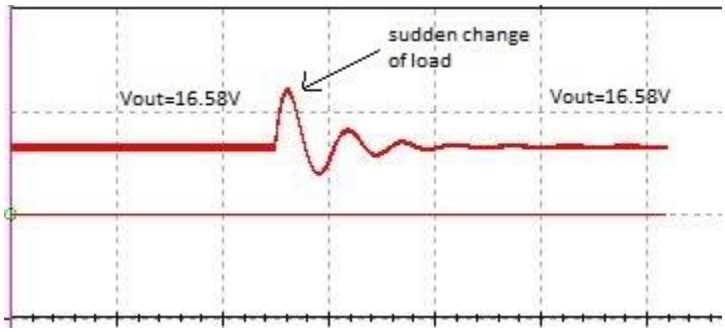

Figure 24. Output response to change in load

The simulation in Figure 23 shows that the output and input satisfy equation (4.3). The responses are very similar to the ones in a buck converter, when a sudden change occurs, i.e. duty ratio or load, the system takes a period of time to become stable again, and the transient response is underdamped with some serious oscillation.

4.3.3 Other DC Converter Topologies

Buck and boost converters are just two most basic topologies for DC/DC power conversion. There are many other topologies to satisfy different demands, this part introduces some alternatives for a microgrid power stage.

4.3.3.1 Buck-Boost Converter

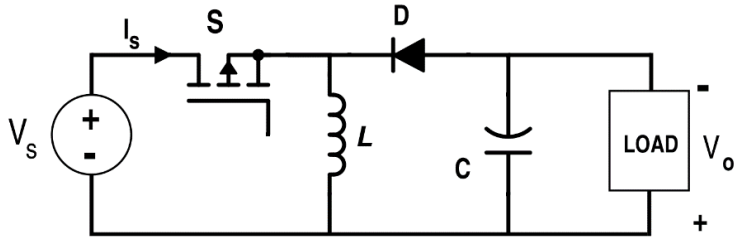

Figure 25. Topology of a buck-boost converter. Source: Figure 25 is from [26].

The buck-boost converter can either step up or step down a DC voltage. The user can adjust its duty ratio to decide whether it will work in buck mode or boost mode. However, its output voltage will be in reversed polarity of the input voltage.

4.3.3.2 Cuk Converter

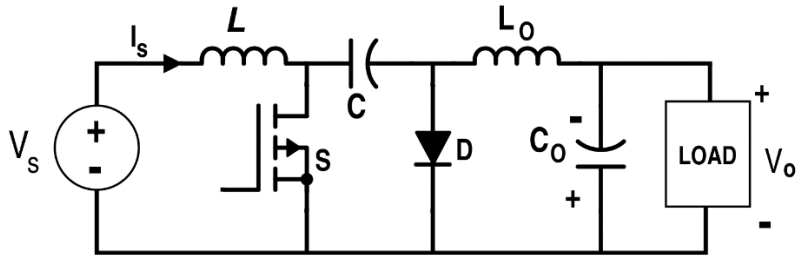

Figure 26. Topology of a Cuk converter. Source: Figure 26 is from [26]

A Cuk converter also has an output voltage magnitude that can be either greater than or less than the input voltage magnitude and has an inverting output. However, it uses an additional set of inductor and capacitor compared to the buck-boost converter. The more complicated design not only reduces harmonics because the inductor at the input side acts as a filter, but also gives a continuous current at the input side, unlike the discontinuous input current in a buck-boost converter.

4.3.3.3 Bi-directional Converter

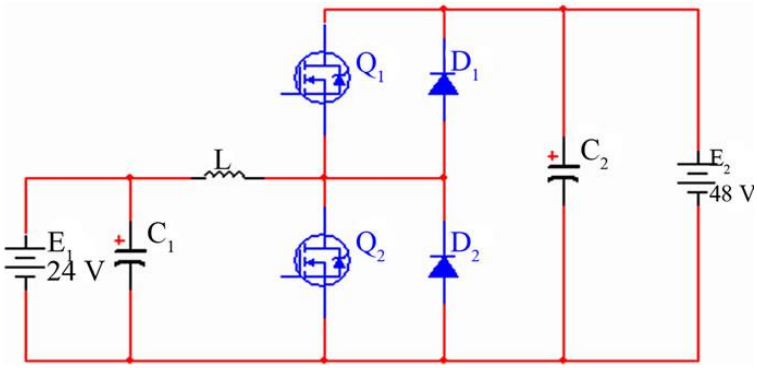

Figure 27. Topology of a bi-directional converter. Source: Figure 27 is from [28]

Figure 27 shows a bi-directional converter with two terminals of E_1 at 24V and E_2 at 48V. When MOSFET Q_2 is driven, power is flowing from E_1 to E_2, the circuit is working as a boost converter. When MOSFET Q_1 is driven, power is flowing from E_2 to E_1, the circuit is working as a buck converter.

The bi-directional converter can be installed between the DC bus and the PHEV battery, since the power flow can be in either direction depending on if the battery is charged by PV or discharges to load.

4.4 DC/AC Converter Models

4.4.1 Rectifier

A rectifier is used to convert AC power into DC power, for example, when the AC bus is charging the PHEV battery in the AC microgrid. In the power adapters of some electronic devices such as a laptop, there is a rectifier in the first power stage to convert AC into DC, then step the DC voltage down to serve the device.

4.4.1.1 Circuit Model

The most commonly seen rectifier is called diode bridge rectifier. These diodes will make current flow in one direction in load, converting AC power into DC. A more advanced design is to replace these diodes with thyristors, which has a gate to receive a firing signal. Upon firing, the forward biased p-n junction will conduct. Figure 28 shows this type of rectifier.

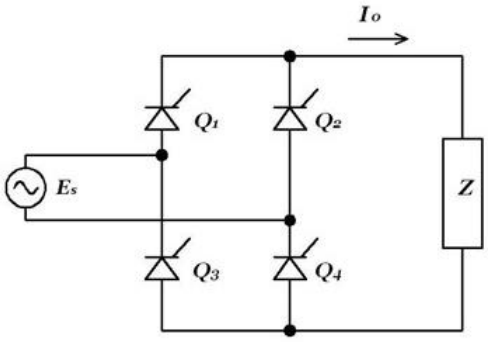

Figure 28. Rectifier with thyristor control

The average output voltage for an RL load is expressed by [29]:

$$V_o = \frac{2V_m}{\pi}\cos(\alpha) \ldots (4.4)$$

where V_m is the peak of input sinusoidal voltage, α is the thyristor firing angle.

4.4.1.2 Rectifier Simulation

The following circuit has been built in Simulink to run the simulation of a thyristor rectifier. During this simulation, the firing angle will be adjusted to $0°$, $60°$ and $120°$ to see its impact on output. The input voltage is 100V peak with a frequency of 50 Hz. In real applications, there is always a filter capacitor at the output to ensure the output a stable DC voltage. In the simulation results, the first graph shows the output voltage with a capacitor filter, the second shows the output voltage without a capacitor and the third shows the input current.

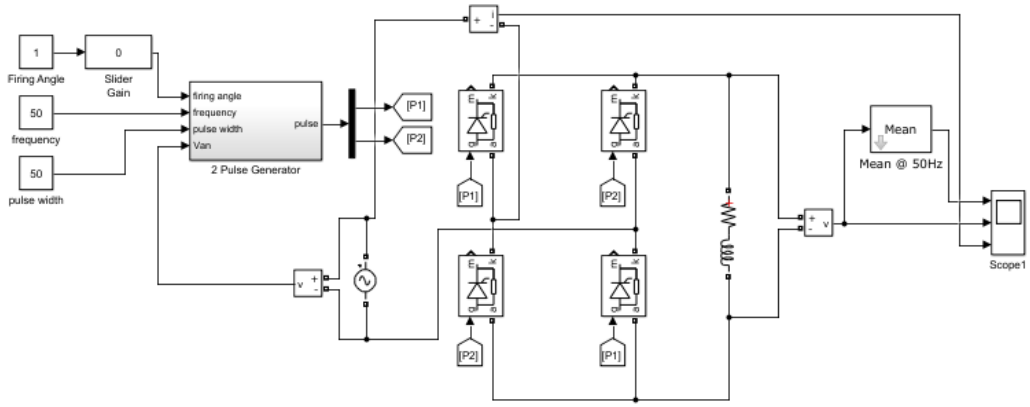

Figure 29. Simulation circuit of a controlled rectifier

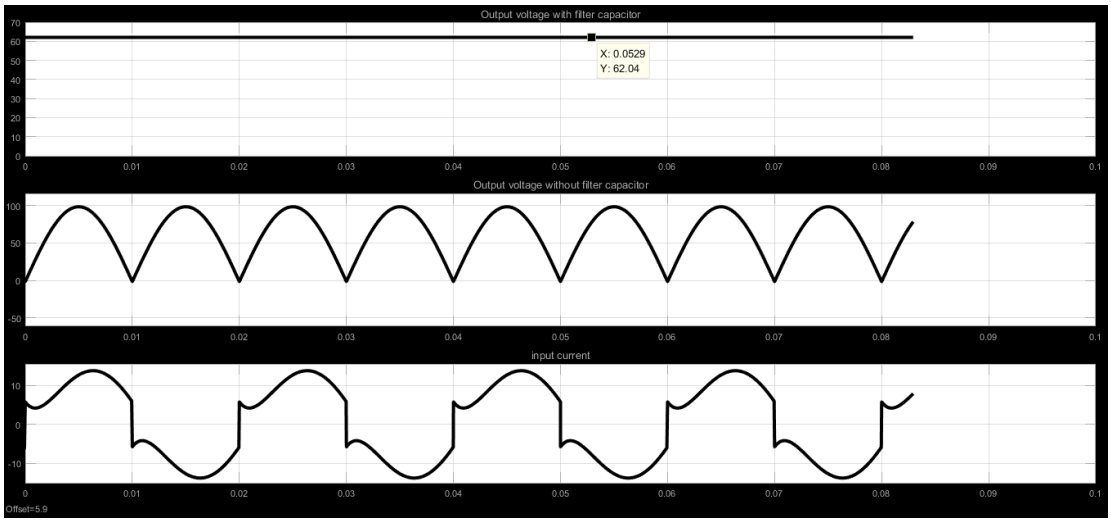

Figure 30. Firing angle at 0°, average output voltage is 62.04V

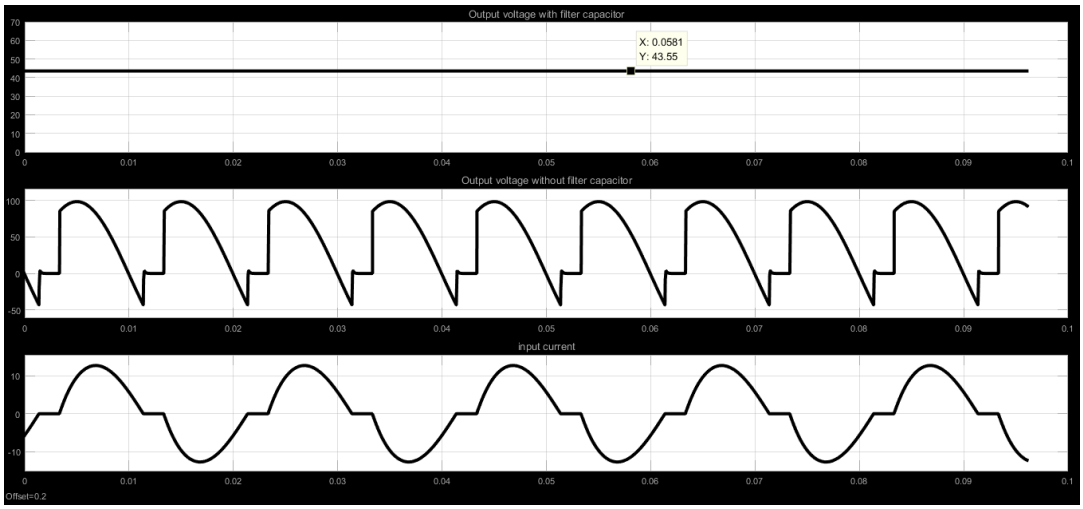

Figure 31. Firing angle at 60°, average output voltage is 43.55V

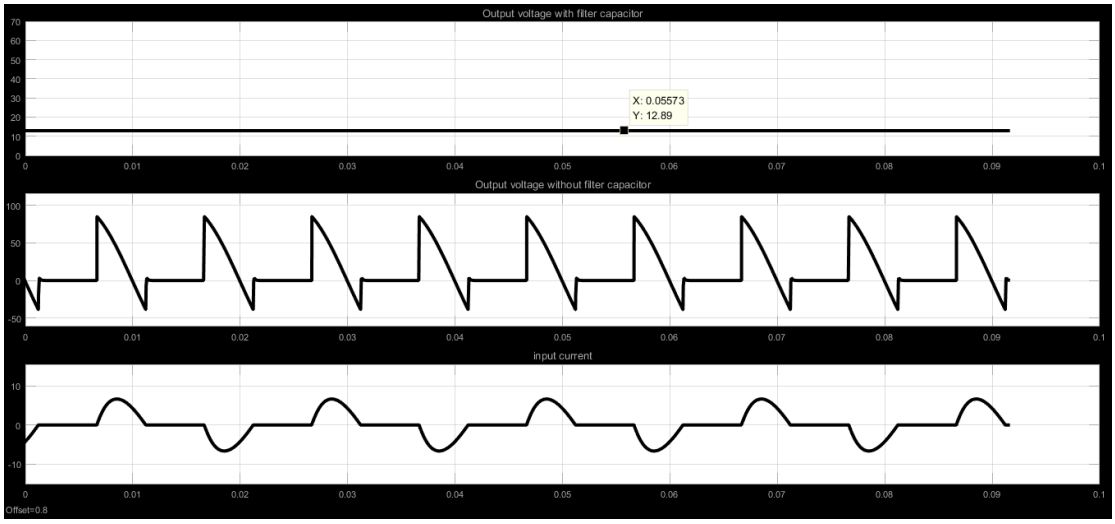

Figure 32. Firing angle at 120°, average output voltage is 12.89V

From these simulations, we can see that the relationship between output voltage and firing angle satisfies equation (4.4). Increasing the firing angle will bring the output voltage down. It is worth noticing that the input current is highly nonlinear, therefore, manufacturers should be very careful with their design because it will inject harmonics

pollutions as well as bringing the power factor down. A rectifier often has a built-in harmonics filter and power factor correction (PFC) circuit.

4.4.2 Power Inverter

A power inverter is used to convert DC power into AC. In a microgrid system, the PV and EV battery need inverters to serve the AC load. Because the application is in a house-level microgrid not an industrial or commercial building, only single phase inverters are investigated in this thesis.

4.4.2.1 Circuit Model

An inverter has a very similar structure as a rectifier, but uses MOSFETs (or IGBTs) instead of diodes. Figure 33 shows a typical circuit model.

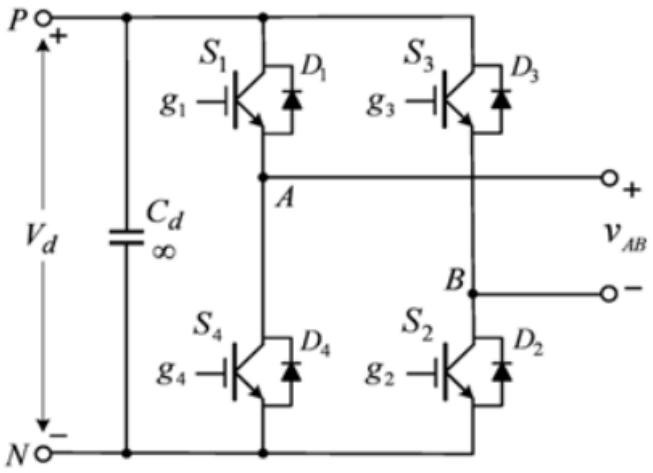

Figure 33. Single phase inverter. Source: Figure 33 is from [30]

The four MOSFETs have some well-designed gate signals to achieve a specific switching pattern. These signals are generated using sinusoidal pulse width modulation (SPWM) which will be introduced in the simulation part. Generally, for three phase

inverters, the gate signals are generated using space vector pulse width modulation (SVPWM); for single phase, signals come from SPWM.

The MOSFETs S1 to S4 will switch a pattern so that during some time, S1 and S2 are on, S3 and S4 are off, load current flows from A to B. Then S3 and S4 are on, S1 and S2 are off, the current flows from B to A. This will create an AC load current. It is also important to make sure that S1 and S4 are not switched on at the same time, as well as S2 and S3, so that the DC source is not shorted.

4.4.2.2 Inverter Simulation

The SPWM switching pattern has two types: unipolar and bipolar. The simulation here uses unipolar switching, which compares a triangular wave with carrier frequency f_c and two sinusoidal waves in reversed phase with modulation frequency f_m. The inverter output voltage $V_{AB} = V_{AN} - V_{BN}$ switches either between zero and $+V_d$ during positive half cycle or between zero and $-V_d$ during negative half cycle of the fundamental frequency, thus this scheme is called unipolar modulation. The modulation index m_a is defined as

$$m_a = \frac{\max |V_m|}{\max |V_{cr}|} \dots (4.5)$$

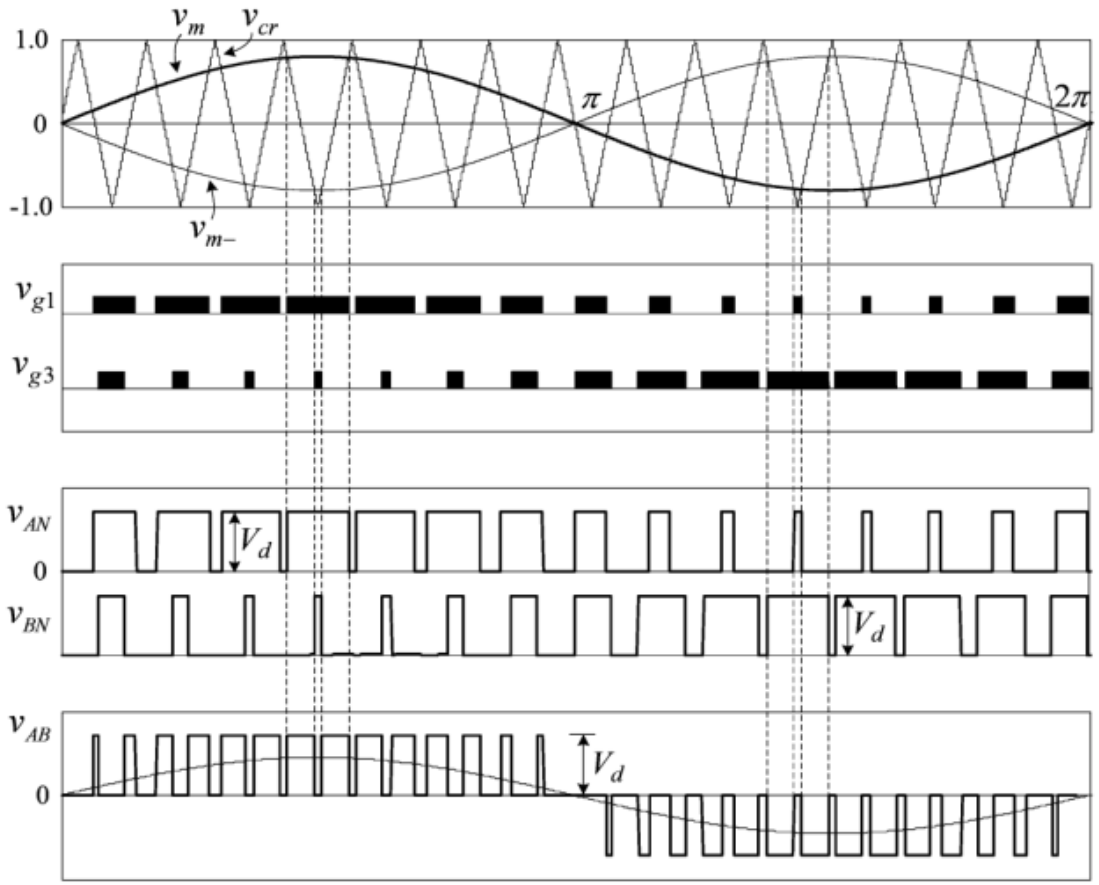

Figure 34. Waveforms of unipolar SPWM. Source: Figure 34 is from [30].

In our simulation, the carrier frequency f_c = 4kHz and the modulation frequency f_m = 60Hz. The input voltage V_d is 50V and the modulation index m_a = 0.8. Figure 35 and 36 shows the output voltage V_{AB} and its frequency analysis.

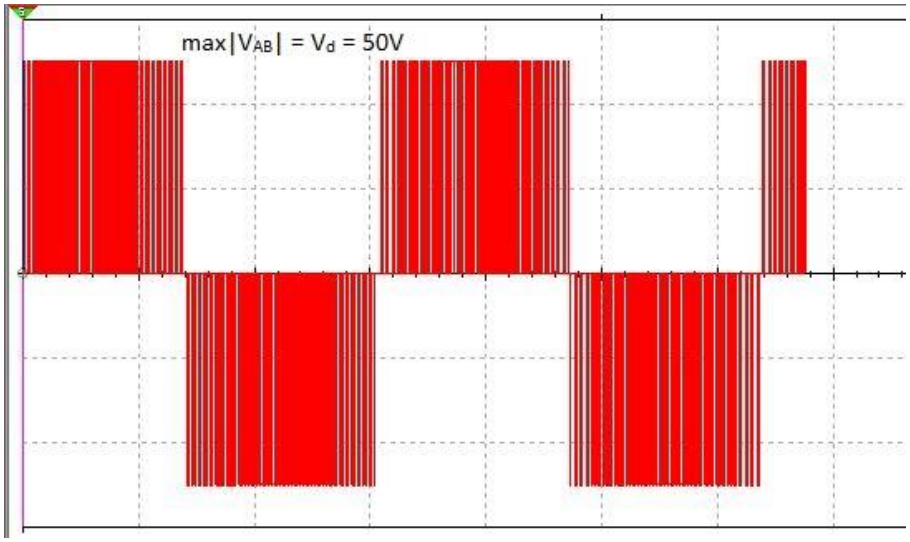

Figure 35. Output voltage V_{AB}

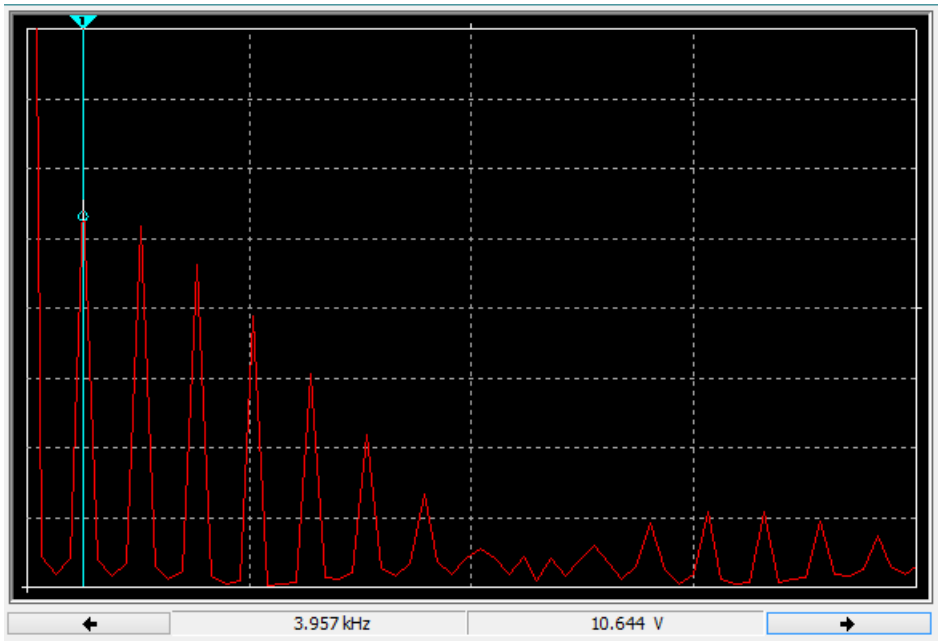

Figure 36. Spectrum analysis of output V_{AB}

From Figure 35, it can be seen that V_{AB} follows the waveform in Figure 34, but since it has a much higher carrier frequency (4kHz) compared to the modulation frequency (60Hz), the pulses look much denser. At frequency domain, the first harmonic

is at approximately 4kHz with an amplitude of 10.6V, which means that a low pass filter with a cut-off frequency less than 4kHz is required. The spectrum analysis shows the advantage of using PWM to generate transistor gate signals: the harmonics have very high frequencies, which makes it easy to filter them out. Figure 37 shows the output voltage after applying an LC low pass filter with the cut-off frequency at 1.06kHz. Figure 38 shows that the first harmonic at 4kHz has been suppressed to 0.8V.

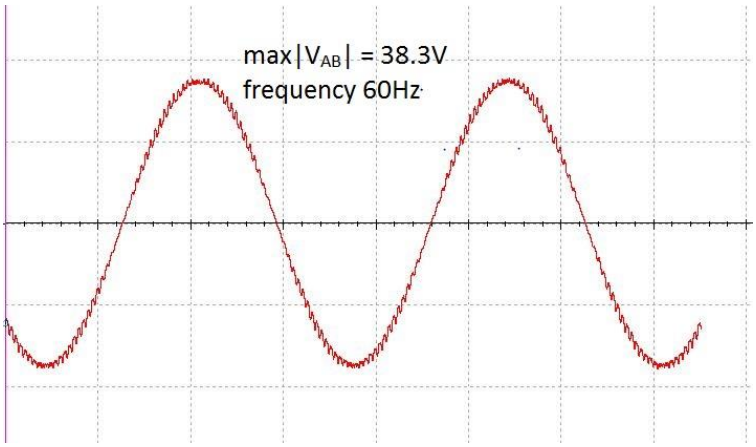

Figure 37. Output voltage V_{AB} with filter

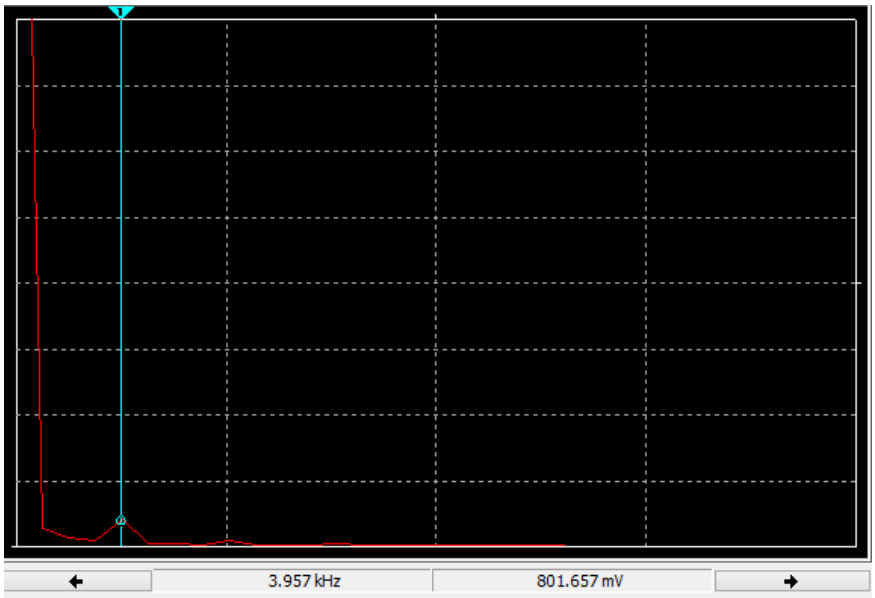

Figure 38. Spectrum analysis of output V_{AB} with filter

The output voltage after the filter is expected to be

$$\max|V_{AB}| = m_a \cdot V_d = 0.8 \cdot 50 = 40V \ldots (4.6)$$

However, the actual voltage is slightly lower than 40V in Figure 37. This is because that dead time is inserted to make sure that two switches on the same leg do not switch on at the same time. During the deadtime, all four switches are off, the power flow from DC to AC is cut off. The dead time insertion will result in some voltage magnitude loss. From the results, we can see that the inverter has successfully converted a DC voltage into a sinusoidal AC. The output voltage can be adjusted by changing the modulation index. In a real power system, a phase locked loop is required to make sure that the connection from a DC generation to an AC bus has the same phase as the distribution line.

Chapter 5 Power Electronics Control in V2H System

5.1 INTRODUCTION

In a microgrid system, there are lots of voltage changes taking place in a house load. For example, when we are using a DC bus to charge a Lithium battery in the customer load, the charging voltage does not stay constant. Figure 39 shows a Li-ion battery charging profile:

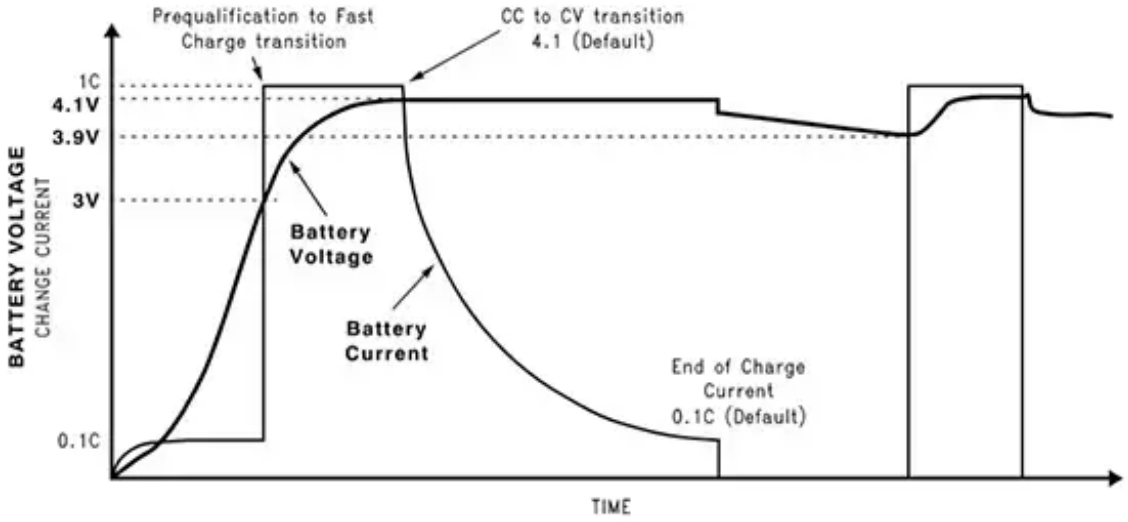

Figure 39. Charging profile of a Li-ion battery. Source: Figure 39 is from [31]

During the charging process, the voltage slowly rises to 4.1V, then stays constant, and fluctuates after it finishes charging.

From the DC/DC converter parts in Chapter 4, we know that in order to change the output voltage, the MOSFET duty ratio needs be changed. However, from the simulations results, it is shown that the transients during a voltage change is very

unacceptable. In this chapter, we will seek the method to change the highly oscillatory transients to a fast and smooth response.

5.2 Introduction to Frequency Compensation

In a feedback control system, a compensator is used to improve an undesirable frequency response. The whole closed-loop feedback control system block diagram is shown in Figure 40.

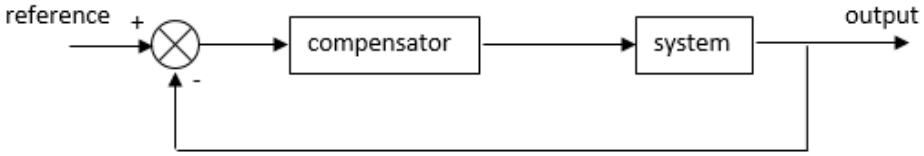

Figure 40. Closed-loop block diagram

Take the following system transfer function for example:

$$G(s) = \frac{40}{s^2 + 2s} \ldots (5.1)$$

The Bode plot of this system is shown in Figure 41:

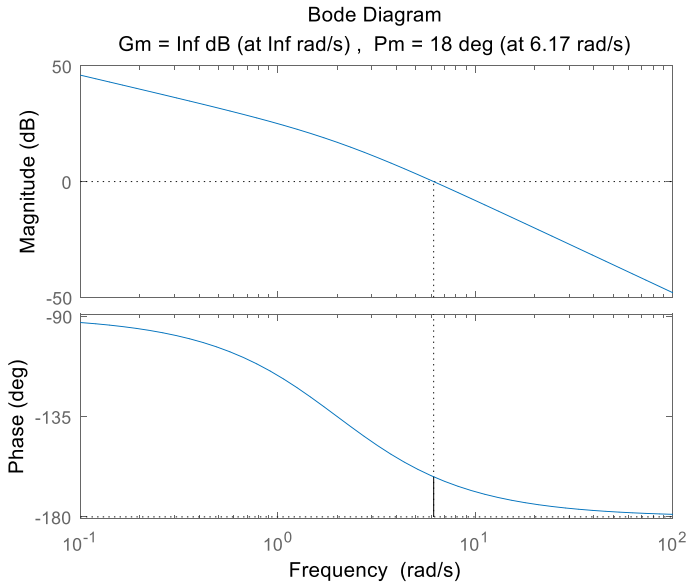

Figure 41. Bode plot of the example system

The phase margin is defined as degrees of phase difference to $-180°$ when the system gain is unity (0dB). For example, when the phase is $-180°$ at unity gain, the phase margin is 0. The closed-loop system will become an oscillator because the output feedback will have the same magnitude but in reversed phase with the input. Therefore, the phase margin defines how far the closed-loop system is to instability. If the phase margin is small, the system is close to instability, so the system response will be highly oscillatory. In order to have a responsive and smooth output, we need to design compensators to keep the system phase margin within a reasonable range.

From Figure 41, it is shown that the phase margin P_m is $18°$, which is not an acceptable margin since, in practice, component tolerance or other variations could make the margin zero. The step response of the closed-loop system in Figure 42 also demonstrates the effects of a small phase margin.

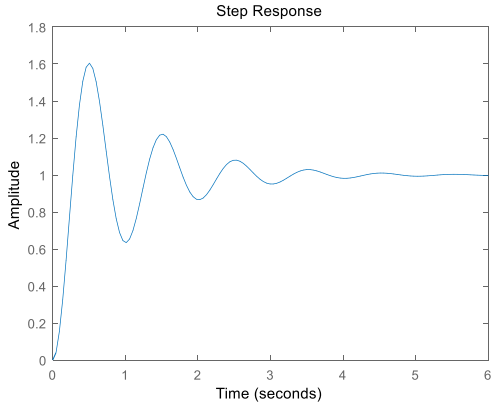

Figure 42. Closed-loop step response when phase margin is $18°$

From Figure 42, it is shown that the response has a 60% overshoot with oscillation. It takes the system 5 to 6 seconds to reach steady state. In some applications,

a slow and oscillatory response like this is not acceptable. If the following compensator is introduced:

$$C(s) = 4.2 \cdot \frac{s + 4.35}{s + 18.11} \ldots (5.2)$$

The Bode plot of the system with compensation is shown in Figure 43, with a phase margin of $50.3°$.

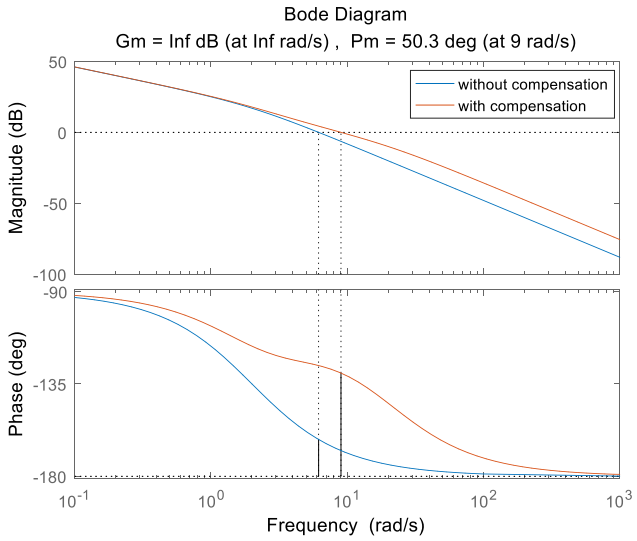

Figure 43. Bode plot comparison of system with and without compensation

From the Bode plot, it is shown that the phase margin has been boosted by a large portion, from $18°$ to $50.3°$. The frequency at which the system has unity gain, also called crossover frequency, has shifted to the right. This indicates that the system can respond to a higher frequency, thus is less immune to noise.

Figure 44 compares the two closed-loop step responses.

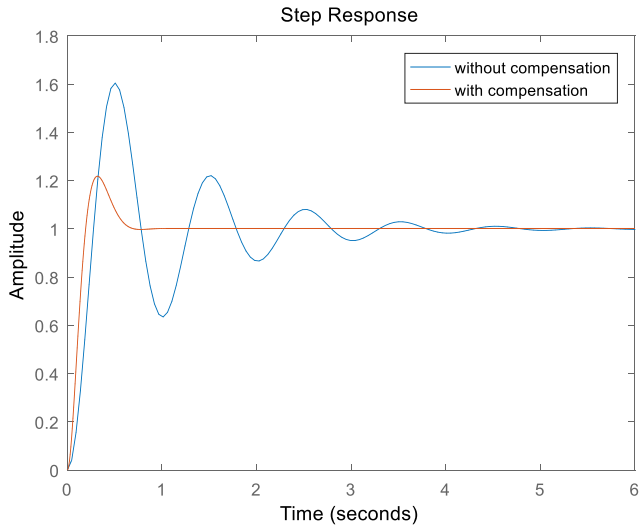

Figure 44. Closed-loop step response

From this figure, it is shown that the overshoot has decreased from 60% to 20%, and the response time is within 1 second, which is much faster than the response without the compensator.

5.3 Compensator Types

In the previous part, an example of closed-loop control with compensators has been introduced. In general, the design criteria are defined by the crossover frequency and its phase margin. Based on the expectations of different applications, the design of compensator varies. In general, compensators are grouped into three types: lead compensator, lag compensator and lead-lag compensator.

5.3.1 Lead Compensator

The compensator C(s) used in part 5.2 is a lead compensator. For a general lead compensator, the transfer function is

$$C(s) = \frac{1 + \alpha Ts}{1 + Ts} \quad (\alpha > 1) \ldots (5.3)$$

Some designers also use a general transfer function of

$$C(s) = K\frac{s - z_0}{s - p_0} \ldots (5.4)$$

These two representations are equivalent. (5.4) represents the transfer function in terms of its gain, pole and zero. The gain $K = \alpha$, the pole $p_0 = -\frac{1}{T}$ and the zero $z_0 = -\frac{1}{\alpha T}$. Since $\alpha > 1$, the pole will be on the left of the zero. In the example compensator in equation (5.2), the pole is at -18.11 rad/s and the zero is at -4.35 rad/s. So, the corresponding $\alpha = 4.2,\ T = 0.055$. The Bode plot of the compensator is shown as

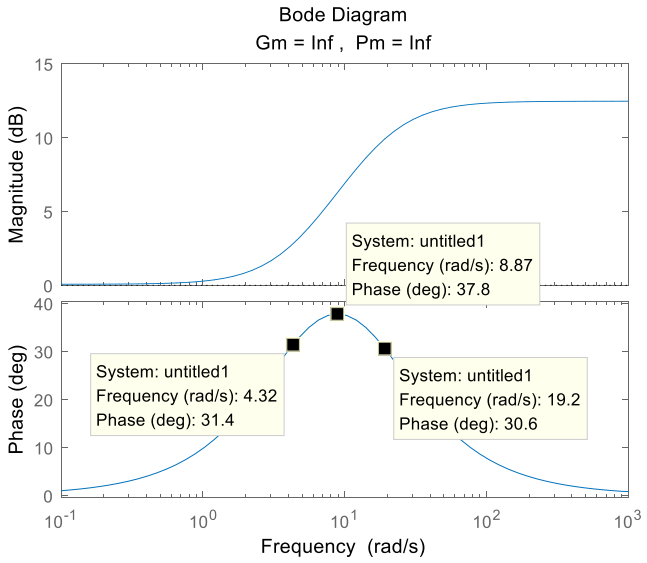

Figure 45. Bode plot of the lead compensator

Figure 45 shows that the positive phase is added to the system between these two frequencies. The maximum amount of phase is added at the center frequency, which is calculated according to equation (5.5).

$$w_m = \frac{1}{T\sqrt{\alpha}} \ldots (5.5)$$

The w_m here is calculated as 8.87 rad/s, which is the same as the frequency shown in the plot. The maximum phase boost can be calculated by the equation below:

$$\emptyset = sin^{-1}\left(\frac{\alpha - 1}{\alpha + 1}\right) \ldots (5.6)$$

The $\emptyset$ here is calculated as $38°$, which is very close to the $37.8°$ phase boost in the plot. The process of designing a lead compensator is to determine α from the phase margin requirements, then determine T to place the added phase at a desired crossover frequency.

It is also worth noticing that the gain at low frequency is kept unity, so the system steady state response will not be affected much. However, the gain at high frequency has been raised by the compensator. This will increase the system crossover frequency, increase the transient response speed, but reduce noise immunity. These trade-offs need to be considered in a design.

5.3.2 Lag Compensator

A lag compensator has an opposite impact to a lead compensator. The general function for a lag compensator can be written as:

$$C(s) = \frac{1}{\alpha}\left(\frac{1+\alpha Ts}{1+Ts}\right) \quad (0 < \alpha < 1) \ldots (5.7)$$

The transfer function can also be written in the form of equation (5.4), but with the pole on the right of the zero. The main difference is that the lag compensator adds negative phase to the system over the specified frequency range, while a lead compensator adds positive phase.

Figure 46 shows the Bode plot for a lag compensator $C(s) = \frac{s+0.503}{s+0.082}$

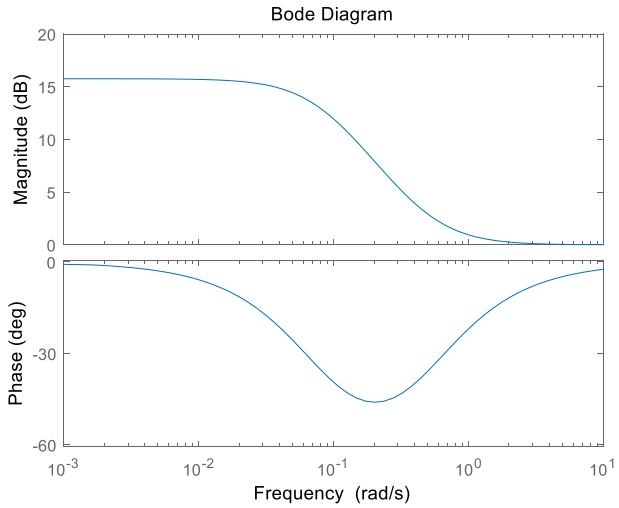

Figure 46. Bode plot for a lag compensator

It can be confusing that since a higher phase margin gives a better response, what is the reason to add a lag compensator to the system. In fact, the phase lag it brings is a side effect of its benefits: to improve the system steady state response. From the magnitude plot, the gain at low frequency is amplified by a factor of $\frac{1}{\alpha}$ $(0 < \alpha < 1)$, leading to the reduction of steady state error (the error between output and reference input when output stays constant) by a factor of $\frac{1}{\alpha}$. The gain at high frequency is unity, therefore the transient response time will not be impacted much.

Figure 47 and 48 show the Bode plot and closed-loop step response of the of the system $G(s) = \frac{1}{(s+1)(s+4)}$ with the compensator in Figure 46.

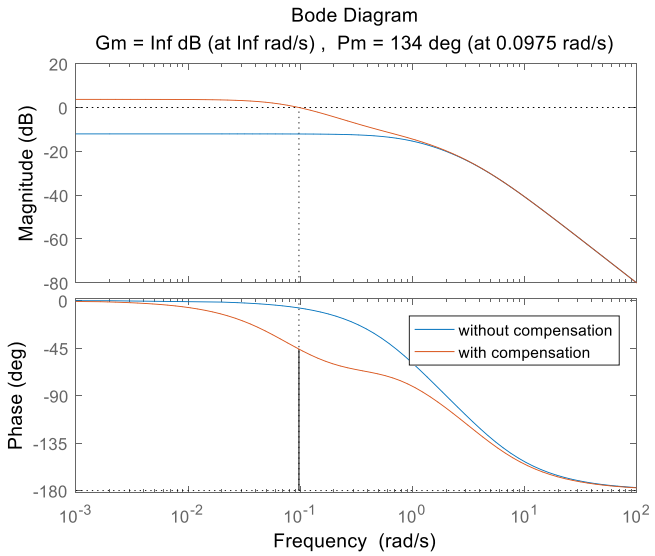

Figure 47. Bode plot comparison of system with and without compensation

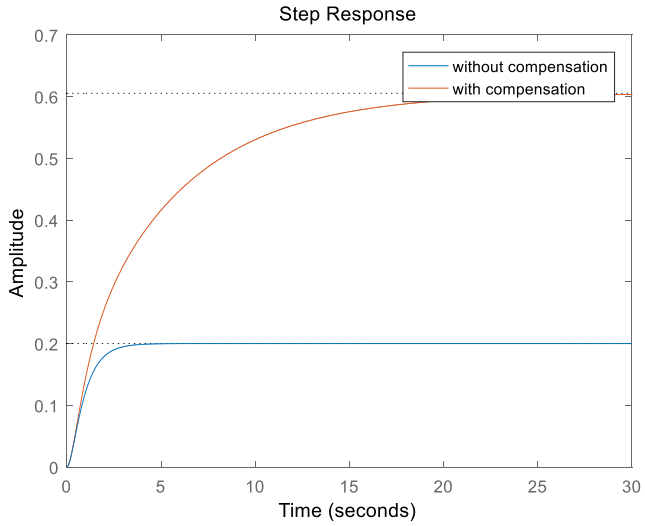

Figure 48. Closed-loop step response

In Figure 47, for the compensated system, the phase becomes closer to the $-180°$ limit, but the magnitude becomes higher at low frequencies. The impacts are clear in Figure 48: after applying the lag compensator, the closed-loop response becomes slower than before, but the steady state error has dropped from 80% to 40%.

Overall, the trade-offs to consider in a lag compensator design is that the potentially lowered phase margin will make system have a less satisfactory transient response, become closer to instability, but have a smaller steady state error.

5.3.3 Lead-lag Compensator

In previous parts, the design rule introduced can be summarized as the following:

- To improve the system transient response, i.e. the phase margin, response time and oscillations, we need a lead compensator.
- To improve the system steady state response, i.e. the steady state error, we need a lag compensator.

However, in some applications, it is required to have not only a fast and smooth transient response, but also a negligible steady state error. A lead-lag compensator is a compensator that combines the advantages of both compensators. The general transfer function of a lead-lag compensator can be expressed as:

$$C(s) = K\frac{1+sT_1}{1+\alpha sT_1}\frac{1+sT_2}{1+\beta sT_2} \dots (5.8)$$

where $\beta > 1, 0 < \alpha < 1, T_1 < T_2$.

The Bode plot of an example lead-lag compensator $C(s) = 10\frac{(s+100)(s+0.1)}{(s+1000)(s+0.01)}$ is shown in Figure 49:

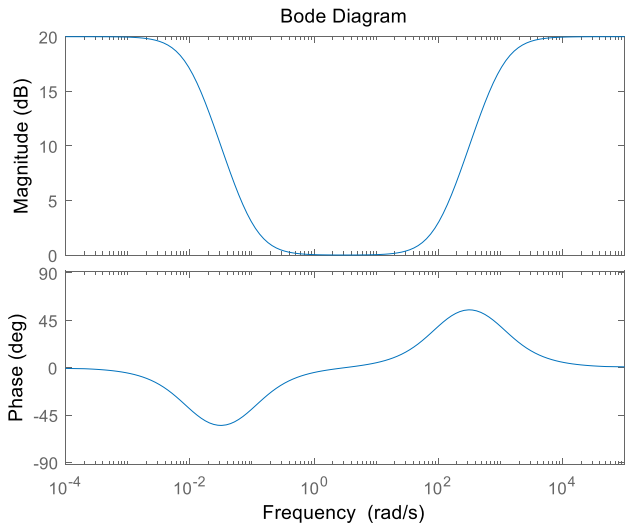

Figure 49. Bode plot of a lead-lag compensator

In this figure, at low frequency, the lag compensator becomes effective to improve the system steady state response; at high frequency, the lead compensator takes over to improve the system transient response.

5.4 Control Application in Power Electronics

The control block diagram for a voltage control mode DC/DC converter is shown in Figure 50:

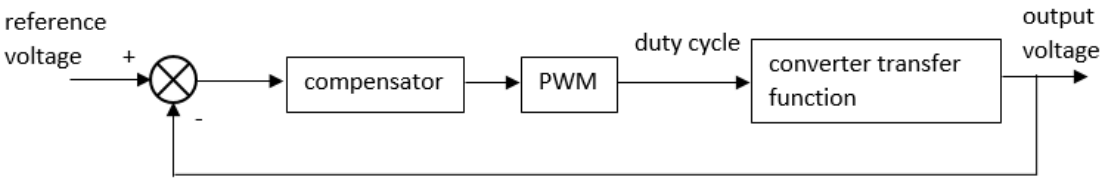

Figure 50. Closed-loop control of a DC/DC converter

The PWM simply converts the compensated error linearly into the duty cycle of MOSFET gate-driving PWM signals. Thus, the converter transfer function and compensator design need to be studied.

5.4.1 Converter Transfer Function

For different types of converters, the transfer function varies. In a general case, the input voltage remains constant, so the transfer function is built between the input duty cycle of MOSFET gate driver and the output voltage. Unlike the relationships given by equation (4.2) and (4.3) where voltage and duty cycle are discussed in a sense of average, to study the transient response, we need to look at the small signal model of the converter due to the presence of a nonlinear MOSFET switch.

A buck converter will be studied in this part because it is most likely to supply batteries, LEDs and other loads that require a varied voltage using a buck converter. The circuit topology can be found at Figure 17:

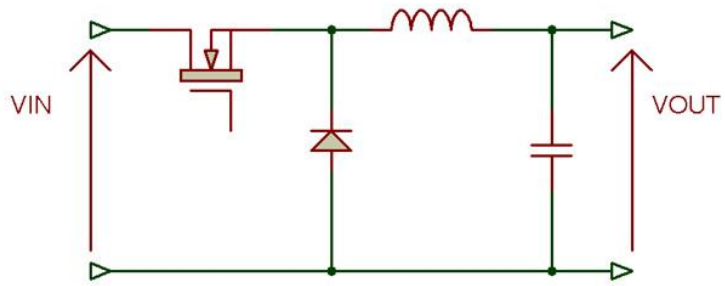

Figure 17. Topology of a basic buck converter. Source: Figure 17 is from [25]

Suppose the duty ratio is D, input voltage is V_{in}, output voltage is V_{out}, output current is I_{out}, inductor is L, capacitor is C, output is a resistor R, current through L is I_L, current through C is I_c. The small signals are represented by lower case symbols.

When the switch is on at cycle D, there is this relationship:

$$L\frac{dI_L}{dt} = V_{in} - V_{out} \quad \ldots (5.9)$$

And when switch is off at cycle (1-D), we have

$$L\frac{dI_L}{dt} = -V_{out} \quad \ldots (5.10)$$

In average, the inductor current satisfies

$$L\frac{dI_L}{dt} = D(V_{in} - V_{out}) + (1-D)(-V_{out}) = DV_{in} - V_{out} \ldots (5.11)$$

For the small signal inductor current:

$$L\frac{d(I_L + i_L)}{dt} = (D+d)(V_{in} + v_{in}) - (V_{out} + v_{out})$$

$$= DV_{in} + Dv_{in} + dV_{in} + dv_{in} - (V_{out} + v_{out}) \ldots (5.12)$$

(5.12) – (5.11) gives

$$L\frac{di_L}{dt} = Dv_{in} + dV_{in} + dv_{in} - v_{out} \ldots (5.13)$$

Since V_{in} is constant, its small signal $v_{in} \to 0$, (5.13) becomes

$$L\frac{di_L}{dt} = dV_{in} - v_{out} \ldots (5.14)$$

The small signal current in inductor satisfies

$$i_L = \frac{v_{out}}{R} + i_c = \frac{v_{out}}{R} + C\frac{dv_{out}}{dt} \ldots (5.15)$$

Plug (5.15) into (5.14) yields

$$\frac{L}{R}\frac{dv_{out}}{dt} + LC\frac{d^2v_{out}}{dt^2} = dV_{in} - v_{out} \ldots (5.16)$$

Assuming zero initial condition, and take the Laplace transform of (5.16) gives

$$\left(LCs^2 + \frac{L}{R}s + 1\right)v_{out}(s) = d(s)V_{in} \ldots (5.17)$$

The transfer function G(s) then can be derived as

$$G(s) = \frac{v_{out}(s)}{d(s)} = \frac{V_{in}}{\left(LCs^2 + \frac{L}{R}s + 1\right)} \ldots (5.18)$$

This transfer function gives the transient relationship between a change in duty cycle and the corresponding change in output voltage. Consider the following parameters: $V_{in} = 10V, L = 0.5mH, C = 0.5mF, R = 2\Omega$.

The system becomes

$$G(s) = \frac{10}{2.5\times10^{-7}s^2 + 2.5\times10^{-5}s + 1} \ldots (5.19)$$

Figure 51 and 52 show the Bode plot and closed-loop step response of this buck converter.

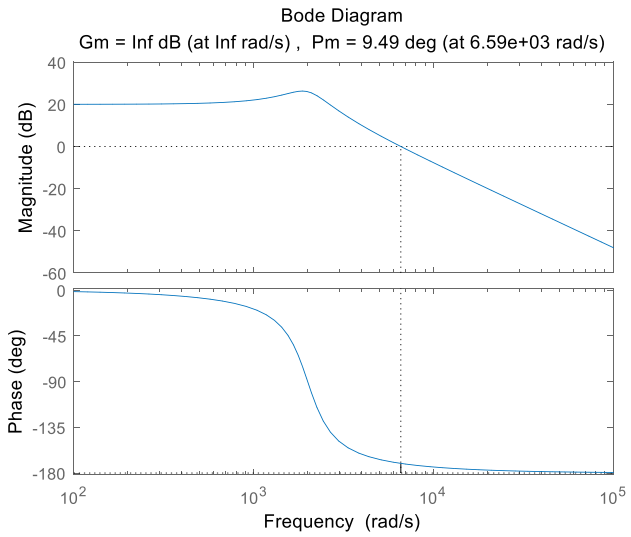

Figure 51. Bode plot of example buck converter

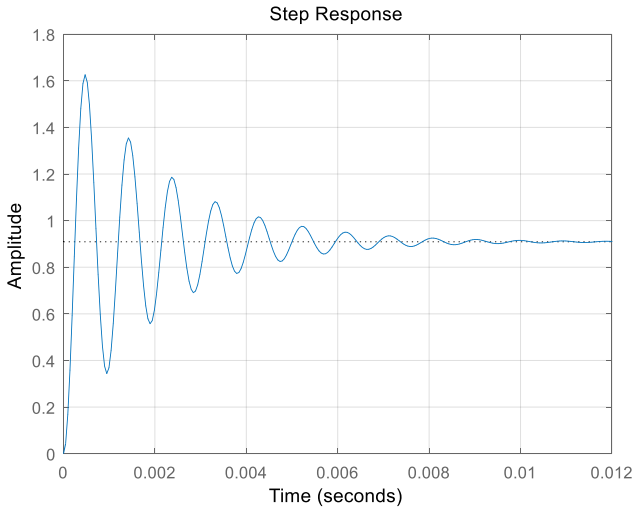

Figure 52. Closed-loop step response of example buck converter

The buck converter has a phase margin of $9.49°$ which has caused unacceptable oscillation and an overshoot of 60%, the response time is roughly 0.01s which is good enough, and the steady state error is 10%.

5.4.2 Lead-lag Compensator Design

First, we design a lead compensator to increase its phase margin. The crossover frequency is at 6.7×10^3 rad/s, and we add a $50°$ phase boost to the system. From equation (5.6), α_{lead} can be calculated as 7.548. We inject the $50°$ phase boost at the crossover frequency, however, since a lead compensator will increase the system crossover frequency, it is better to put the phase boost at a higher frequency, for example at 1×10^4, then from equation (5.5), T_{lead}can be calculated as 3.64×10^{-5}. The lead compensator is designed as

$$C_{lead} = \frac{2.747\times10^{-4}s + 1}{3.64\times10^{-5}s + 1} \dots (5.20)$$

With the transient response improved, the next is the steady state response. Suppose we decrease the steady state error by a factor of 7.548, so $\frac{1}{\alpha_{lag}} = 7.548, \alpha_{lag} = 0.132$. Let $T_{lead} = 0.002$, so from equation (5.5), the phase lag will be injected at 1374 rad/s. Since in the original system, the phase margin at this frequency is very robust, the design of lag compensator is reasonable. The transfer function is written as

$$C_{lag} = \frac{2.64\times10^{-4}s + 1}{2.64\times10^{-4}s + 0.132} \dots (5.21)$$

Then the lead-lag compensator can be written as

$$C_{lead-lag} = C_{lead}C_{lag} \dots (5.22)$$

Figure 53 shows the frequency response of this compensator:

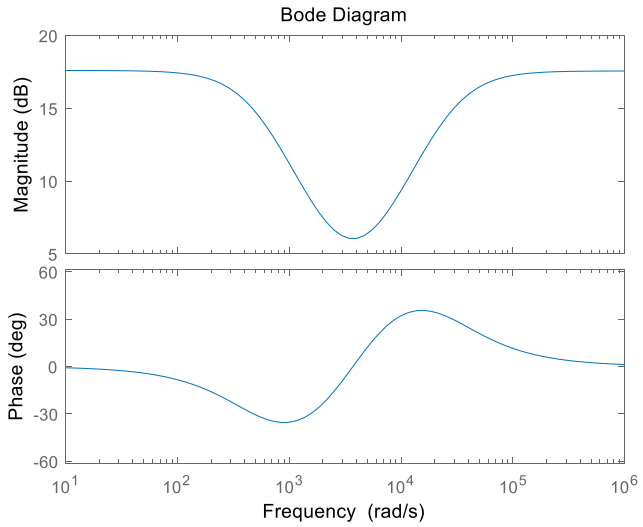

Figure 53. Bode plot of the lead-lag compensator

5.4.3 Buck Converter Closed-loop Simulation

Suppose the duty cycle of the buck converter is 0.5, therefore the output voltage is 5V. A step input in reference voltage means that the reference voltage is increase from 5V to 6V, and the output voltage will follow the reference to increase in a closed-loop. Figure 54 compares the frequency response to the original system without compensation.

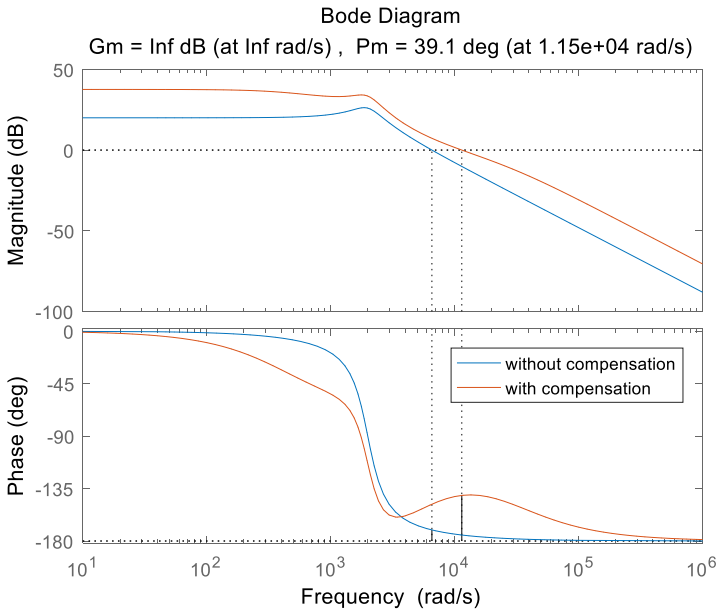

Figure 54. Bode plot of system with and without compensation

From Figure 54, it is shown that the 50° maximum phase boost has not been fully used to improve the phase margin, this is mainly because of the introduction of lag compensator.

Figure 55 demonstrates the voltage regulation process from 5V to 6V, with comparison to the regulation without compensation.

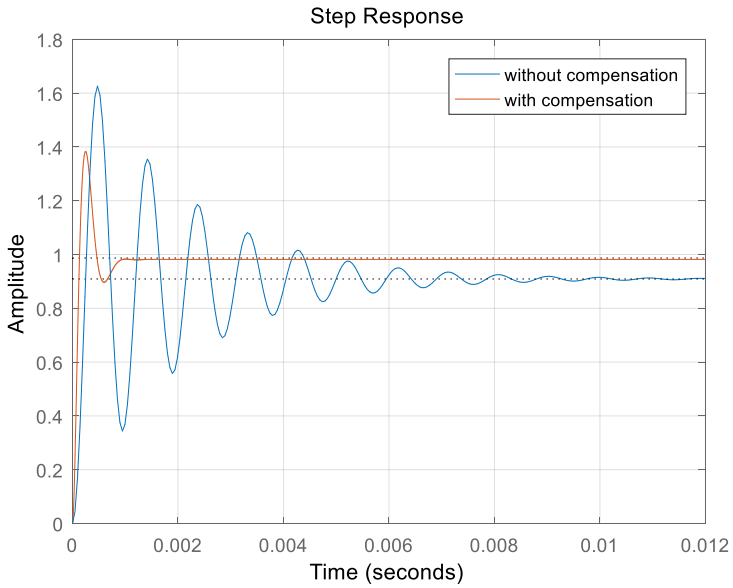

Figure 55. Closed-loop response of system with and without compensation

The result in Figure 55 shows that the overshoot has been reduced from 60% to 40%, the response speed is 10 times faster, and the steady state error can barely be noticed. If it is required to further reduce the overshoot, the lead compensator could be designed to provide a higher phase boost.

5.5 HARDWARE IMPLEMENTATIONS

Compensators can be built from operational amplifiers with resistors and capacitors, for example, the circuit in Figure 56 can be used as a lead compensator. The control signal is processed in analog form.

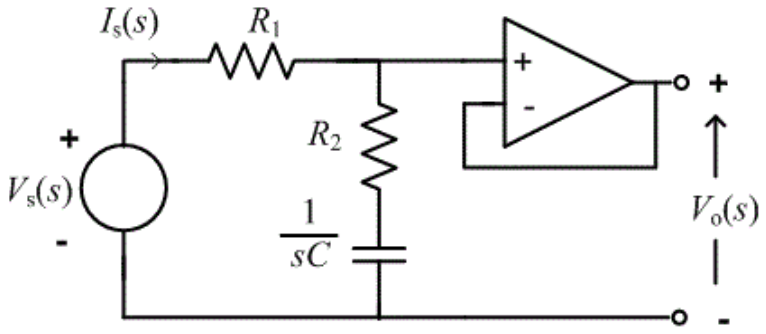

Figure 56. Lead compensator circuit. Source: this figure is from [32]

Modern power electronics are usually controlled in digital form, most commonly seen controllers are programmed into microcontrollers, digital signal processors (DSP) or field-programmable gate arrays (FPGA). To design a digital compensator, the transfer function should be converted from Laplace domain into a different domain by z-transform, and then written into difference equations in a sampling pattern.

Chapter 6 Thesis Summary

6.1 Conclusions

This thesis studied household microgrids and their power electronics. The thesis started with a comprehensive background study into microgrid, followed by motivations and objectives. The first focus was the investigations into a V2H microgrid, with details presented for PHEVs and PV panels. Subsequently, a simulation with data from Pecan Street has illustrated that the set-up of a V2H microgrid with PV is able to maintain a normal house load for a decent number of days throughout the year. Furthermore, the power electronics interfaces for both a DC and an AC microgrid has been introduced, with basic circuit topologies and simulations for different power converters. In the last chapter, the control methods for power electronics have been introduced, and a design example was demonstrated with simulation. The controller has successfully improved the system response as expected.

6.2 Future Work

Due to timing issues, there are still some further aspects remaining to be covered and investigated. These future works may involve:

- Running simulations for the V2H microgrid using more sets of residential house data
- Measuring the power electronics efficiencies for a more accurate V2H system model
- The PV spillage in simulation gets very large during some days, so a new algorithm can be designed to lower PV spillage
- Design compensators for more converter topologies and run simulations

- Compare the influence of using a lead-lag compensator to a PID controller

References

[1] United States Environment Protection Agency (EPA), Cleaner Power Plants, available online: https://www3.epa.gov/mats/powerplants.html

[2] N. Jenkins, R. Allan, P. Crossley, D. Kirschen, and G. Strbac, Embedded Generation, The Institution of Electrical Engineers, UK, 2000.

[3] Degner T, Schmid J, Strauss P. (eds). DISPOWER—Distributed Generation with High Penetration of Renewable Energy Sources. ISET: Kassel, 2006; 11–17.

[4] R.H.Lasseter, MicroGrids, Power Engineering Society Winter Meeting, 2002. IEEE (Volume:1).

[5] Alexis Kwasinski, Grid-Microgrids Interconnection, 2012.

[6] Keiichi Hirose, Toyonari Shimakage, James T. Reilly, Hiroshi Irie, The Sendai Microgrid Operational Experience in the Aftermath of the Tohoku Earthquake: A Case Study, 2013 NEDO.

[7] David P.Tuttle, Robert L. Fares, Ross Baldick, Michael E. Webber, Plug-In Vehicle to Home (V2H) Duration and Power Output Capability, 2013 IEEE.

[8] John D. Herbst, Angelo L. Gattozzi, A. Ouroua, Fabian M. Uriarte, Flexible Test Bed for MVDC and HFAC Electric Ship Power System Architectures for Navy Ships, 2011 IEEE.

[9] Ahmed T. Elsayed, Ahmed A. Mohamed, Osama A. Mohammed, DC Microgrids and Distribution Systems: An Overview, 2013 IEEE.

[10] Mansour Tabari, Amirnaser Yazdani, A DC distribution system for power system integration of Plug-In Hybrid Electric Vehicles, 2013 IEEE.

[11] Fred Wang, Yunqing Pei, Dushan Boroyevich, Rolando Burgos, Khai Ngo AC vs. DC distribution for off-shore power delivery, 2008 IEEE.

[12] Qing-Chang Zhong, George Weiss, Synchronverters: Inverters That Mimic Synchronous Generators, 2011 IEEE.

[13] Daniel Salomonsson, Lennart Soder, Ambra Sannino, Protection of Low-Voltage DC Microgrids, 2009 IEEE.

[14] Joon-Young Jeon, Jong-Soo Kim, Gyu-Yeong Choe, Byoung-Kuk Lee, Jin Hur, Hyun-Cheol Jin, Design guideline of DC distribution systems for home appliances: Issues and solution, 2011 IEEE.

[15] Lianxiang Tang, Boon-Teck Ooi, Locating and Isolating DC Faults in Multi-Terminal DC Systems, 2007 IEEE.

[16] L. Roggia, L. Schuch, C. Rech, H. L. Hey, J. R. Pinheiro, Design of a Sustainable Residential Microgrid System with DC and AC Buses Including PHEV and Energy Storage Device, 2011 IEEE.

[17] U.S Department of Energy, Where the Energy Goes: Gasoline Vehicles, available online: http://www.fueleconomy.gov/feg/atv.shtml.

[18] Wikipedia, Chevrolet Volt, available online: https://en.wikipedia.org/wiki/Chevrolet_Volt

[19] Theodore Bohn and Hina Chaudhry, Overview of SAE Standards for Plug-in Electric Vehicle, 2012 IEEE.

[20] SAE Unveils Combined Charger System, Plugincars, available online: http://www.plugincars.com/sae-unveils-combined-charger-system-121119.html

[21] K. H. Hussein, I. Muta, T. Hoshino, M. Osakada, Maximum photovoltaic power tracking: an algorithm for rapidly changing atmospheric conditions, IEE Proceedings - Generation, Transmission and Distribution (Volume:142, Issue: 1)

[22] Trishan Esram, Patrick L. Chapman, Comparison of Photovoltaic Array Maximum Power Point Tracking Techniques, IEEE 2007.

[23] Faisal Mohamed, Microgrid Modelling and Simulation, Helsinki University of Technology Control Engineering Laboratory, Figure 6.1.

[24] "Vehicle to Home" Electricity Supply System, available online: Nissan Leaf-to-Home

[25] Buck Converter from electronicdesign.com, available online: buck converter

[26] Analysis of Four DC-DC Converters in Equilibrium, All About Circuits, available online: https://www.allaboutcircuits.com/technical-articles/analysis-of-four-dc-dc-converters-in-equilibrium/

[27] Wikipedia, Boost converter continuous mode, available online: https://en.wikipedia.org/wiki/Boost_converter#Continuous_mode

[28] Ambrosio B. Cultura II, Ziyad M. Salameh, Design and Analysis of a 24 Vdc to 48 Vdc Bidirectional DC-DC Converter Specifically for a Distributed Energy Application, Energy and Power Engineering Vol. 4 No. 5 (2012), Figure 2.

[29] Daniel W. Hart, Power Electronics, Chapter 4 equation (4-30)

[30] Anuja Namboodiri, Harshal S. Wani, Unipolar and Bipolar PWM Inverter, International Journal for Innovative Research in Science & Technology, Volume 1, Issue 7

[31] A Designer's Guide to Lithium (Li-ion) Battery Charging, available online: https://www.digikey.com/en/articles/techzone/2016/sep/a-designer-guide-fast-lithium-ion-battery-charging

[32] Op amp Lead compensator, ECE Tutorials, available online at: http://ecetutorials.com/analog-electronics/lag-and-lead-compensators-using-op-amp/

[33] Hunyoung Shin, Ross Baldick, Plug-In Electric Vehicle to Home (V2H) Operation under a Grid Outage, IEEE Transactions on Smart Grid (Volume: PP, Issue: 99)